The Cryosphere, 18, 2035–2059, 2024
https://doi.org/10.5194/tc-18-2035-2024

The Cryosphere
Open Access
EGU

Lake ice break-up in Greenland: timing and spatiotemporal variability

Christoph Posch, Jakob Abermann, and Tiago Silva

Institute of Geography and Regional Science, University of Graz, 8010 Graz, Austria

Correspondence: Christoph Posch (christoph.posch@edu.uni-graz.at)

Received: 31 July 2023 – Discussion started: 2 August 2023
Revised: 28 January 2024 – Accepted: 22 February 2024 – Published: 30 April 2024

Abstract. Synthetic aperture radar (SAR) data from the Sentinel-1 (S1) mission with its high temporal and spatial resolution allows for an automated detection of lake ice break-up timings from surface backscatter differences across south (S), southwest (SW), and northwest (NW) Greenland ($<71^\circ$ N latitude) during the period 2017 to 2021. Median break-up dates of the 563 studied lakes range between 8 June and 10 July, with the earliest being in 2019 and the latest in 2018. There is a strong correlation between the break-up date and elevation, while a weak relationship with latitude and lake area could be observed. Lake-specific median break-up timings for 2017–2021 increase (i.e., are later) by 3 d per 100 m elevation gain. When assuming an earlier break-up timing of 8 d which corresponds to the observed median variability of ± 8 d, the introduced excess energy due to a changing surface albedo from snow-covered ice surface to water translates to melting 0.4 ± 0.1 m thick ice at the melting point or heating up a water depth down to 35 ± 3 m by 1 K across the entire surface area of each respective lake. Upscaling the results to 100 486 lakes across the S, SW, and NW regions, which correspond to 64.5 % of all lakes or 62.1 % of the overall lake area in Greenland, yields an estimate of 1.8×10^6 TJ additional energy input. This translates to melting 5.8 Gt ice at the melting point or warming 432.3 Gt water by 1 K.

1 Introduction

Lake ice plays an important role in biological, chemical, and physical processes of cold region freshwater (Duguay et al., 2015). Freshwater ice in the Arctic and its response to climate change have a variety of effects on hydrologic, ecological, and socioeconomic systems (Prowse et al., 2011), while climate change is one of the most severe threats to global lake ecosystems (Woolway et al., 2020). The duration of lake ice controls the seasonal heat budget of lakes and may have an effect on both regional climate and weather events (Brown and Duguay, 2010; Duguay et al., 2015). The timings of lake ice freeze-up and break-up, i.e., lake ice phenology, are relevant climate indicators and can be useful for monitoring environmental changes (Adrian et al., 2009; WMO, 2022a). Therefore, lake ice is a parameter of the Essential Climate Variable (ECV) "lakes" and included in monitoring programs such as the World Meteorological Organization (WMO) Global Climate Observing System (GCOS) (WMO, 2022a) and the European Space Agency (ESA) Climate Change Initiative (CCI) (ESA, 2023a). The scientific value of lake research and the important role of lakes for humans sees them incorporated in the United Nations' Sustainable Development Goals no. 6 (Clean Water and Sanitation) and no. 13 (Climate Action) (United Nations, 2015) and an essential component of the United Nations Framework Convention on Climate Change (UNFCCC) and the Intergovernmental Panel on Climate Change (IPCC) (Woolway et al., 2020).

Lake ice freeze-up and break-up are the results of energy surplus or deficit in the energy balance of the lake. The energy exchanges between the ice cover or water surface and the atmosphere are mainly determined by air temperature, precipitation, wind, and radiation. The seasonal changes in solar radiation, however, are the main influence for the overall energy availability to form and decay lake ice cover (Brown and Duguay, 2010). Both a linear and non-linear relation between lake ice break-up timing and air temperature have been established, while stronger correlations with latitude were identified compared to elevation (Magnuson, et

al., 2000; Weyhenmeyer et al., 2004; Williams et al., 2004; Duguay et al., 2006; Korhonen, 2006; Williams and Stefan, 2006; Brown and Duguay, 2010; Jeffries et al., 2012; Imrit and Sharma, 2021).

Satellite remote sensing provides the necessary means to increase the spatial coverage and temporal frequency of ground-based observations of lake ice phenology which have been globally declining since the 1980s (Duguay et al., 2015). Synthetic aperture radar (SAR) backscatter exhibits differences between water and ice due to dielectric properties of the materials (Unterschultz et al., 2009) and therefore allows identifying the phenological state of the lake ice cover. Several studies investigated the evolution, characteristics, and phenology of freshwater ice such as river ice (e.g., Lindenschmidt et al., 2011; Stonevicius et al., 2022) and lake ice (e.g., Wang et al., 2018; Murfitt and Duguay, 2020; Tom et al., 2020; Siles et al., 2022) from radar imagery, while we are not aware of any comprehensive study on lake ice break-up timing across Greenland.

In this study, we explore the potential of utilizing Sentinel-1 (S1) SAR data for identifying temporal and spatial variations in the lake ice break-up across S, SW, and NW Greenland between 2017 and 2021 and assess its latitudinal and vertical gradients. Peripheral lakes in Greenland, i.e., lakes excluding supra- and proglacial lakes, make up approximately 0.7 % of the overall land area or approximately 3 % of the unglaciated area. Therefore, we aim to quantify the additional energy input by estimating excess radiation and energy for a potential earlier lake ice break-up timing from the observed lake ice break-up variabilities.

1.1 Climate in coastal Greenland

Greenland extends for approximately 23° of latitude, with temperature, precipitation, and consequently mass balance rates varying considerably across latitudes and coasts (Westergaard-Nielsen et al., 2020; Hanna et al., 2021; Mankoff et al., 2021; Slater et al., 2021; Box et al., 2023). Due to the semi-permanent Icelandic Low and the rocky landscape, the southeast coast receives particularly high amounts of precipitation (e.g., Ettema et al., 2010; Fettweis et al., 2017). As precipitation rates greatly decrease northward, north Greenland is classified as a polar desert with very shallow snow cover that quickly disappears in the warm season. Temperature also tends to decrease with latitude and is related to snow and radiation conditions. However, other factors shape the coastal climate, such as prominent ocean currents (e.g., east Greenland and North Atlantic current) and sea ice conditions (Westergaard-Nielsen et al., 2020). The west and east coasts also exhibit different topographic features like a topographically complex southeast contrasting with generally rather gentle slopes in southwest or north Greenland (Karami et al., 2017). Nevertheless, both the east and west coasts comprise diverse fjord systems impacting regional climate and local wind conditions. Consequently, the leeward side of these inland mountain systems receive reduced precipitation. Such coast–inland gradients are therefore complex, influencing the distribution of permafrost and freshwater systems (Westergaard-Nielsen et al., 2018; Abermann et al., 2021). While several studies on accumulation rates and rainfall exemplify the general east–west gradient in precipitation focusing on the Greenland Ice Sheet (GIS) (e.g., Shen et al., 2012; Koenig et al., 2016; Box et al., 2023), Bales et al. (2009) include and highlight coastal variability in the snow accumulation. In situ and remote sensing data, as well as polar-adapted climate models, point to a Greenland-wide warming in recent decades, particularly in summer (e.g., Westergaard-Nielsen et al., 2018; Jiang et al., 2020; Hanna et al., 2021). Part of this warming is attributed to more frequent and intense anti-cyclonic conditions in the vicinity of Greenland, leading to advection of relatively warm air masses from low latitudes. Silva et al. (2022) showed that the warming applies to different circulation conditions. As a consequence of atmospheric warming, the ratio of liquid to total precipitation has increased in coastal areas, particularly during summer (e.g., Huai et al., 2022; van der Schot et al., 2023). The Arctic Amplification is more pronounced during the cold season, with coastal temperature warming along the west coast linked with reduced sea ice in Baffin Bay (e.g., Ballinger et al., 2020).

1.2 Background and related studies using SAR for studying lake ice cover

The transmitted pulse of SAR systems interacts with the Earth surface, and only a portion of it is backscattered to the receiving antenna. The amplitude and phase of the backscattered signal depends on the physical (i.e., geometry and roughness) and electrical properties (i.e., permittivity) of the imaged object (Moreira et al., 2013). The reflection, transmission, and absorption of the radar beam at lake ice is governed by the (combination of) interactions with water, ice, snow, and air. The differences in the amplitude of the backscattered signal between ice and water due to the influence of the electrical properties (Unterschultz et al., 2009) can be utilized to identify the phenological state of the ice cover of lakes.

Using satellite data for studying lake ice possesses several advantages over ground observations in terms of data availability and accessibility. Ground observations of lake ice may be limited due to access to remote and unpopulated areas and safety hazards during freeze-up and break-up periods. Satellite observations are independent from these restrictions and offer a relatively rapid, lower-cost, and spatially broader way of obtaining data (Siles et al., 2022). Radar is independent from daylight and weather conditions, and S1 SAR data are available and accessible at high spatial and temporal resolutions (ESA, 2023b). Lake ice studies from remote sensing can produce results and extrapolate field measurements across large spatial scales as opposed to field studies based

on a small number of ground observations. However, field observations are pivotal for validation purposes (Murfitt and Duguay, 2021).

Wang et al. (2018) utilized dual polarized RADARSAT-2 imagery for a semi-automated, pixel-by-pixel ice vs. water classification at Lake Erie and provided an overall accuracy of up to 90.4 %. Using a deep learning network, Tom et al. (2020) conducted a pixel-based lake ice phenology classification from S1 SAR data for three alpine lakes in Switzerland and found accuracies well above 90 %. They demonstrated that the phenological state of the lake ice cover of non-transition days (i.e., ice/snow or water) can be identified confidently. Murfitt and Duguay (2020) utilized S1 high-density time series data to monitor ice phenology of the High Arctic Lake Hazen (Canada) and demonstrated mean errors between 3 and 7 d when identifying the timing of lake ice break-up. Since it has been demonstrated that lake ice phenology can be assessed using SAR data, we develop a dynamic numerical threshold to automatically identify the lake ice break-up timing from SAR backscatter across Greenland.

2 Data

2.1 Greenland lake inventory

The Greenland lake inventory (Styrelsen for Dataforsyning og Infrastruktur, 2023a) includes 155 870 peripheral lakes in Greenland ranging from 1.6×10^{-3} to 138 km^2. The vector data set is part of the data inventory Databoks Grønland (Styrelsen for Dataforsyning og Infrastruktur, 2023b) and based on commercial satellite images with a resolution of 0.5 m primarily from summer months in the period from 2017 to 2021.

2.2 Sentinel-1 SAR

The Sentinel-1 mission consists of satellites S1A and S1B which acquire C-band SAR data with a center frequency of 5.407 GHz (ESA, 2023c). Single-polarized horizontal transmit/horizontal receive (HH) Level-1 ground-range-detected (GRD) data in both ascending and descending orbit acquired in Interferometric Wide (IW) swath mode with a swath width of 250 km is used in this study (ESA, 2023b). The HH polarization and IW swath mode are chosen due to the comprehensive spatial coverage of Greenland. The satellites have near-polar, sun-synchronous orbit with a 12 d repeat cycle and 175 orbits per cycle for each satellite. S1A and S1B have the same orbit plane with a 180° orbital phasing difference which results in an actual repeat cycle of 6 d with both satellites operating (ESA, 2023b). To determine the timing of lake ice break-up, it is crucial to utilize the highest possible temporal resolution of the SAR data, which is why we use data from both ascending and descending orbits. The combination of both orbital modes and the high overlap of the acquisitions due to converging orbits close to polar regions leads to a coverage with a revisit frequency of below 2 d for most of Greenland (ESA, 2023b). Our study period is constrained to 2017–2021 since we require both satellites being operational to ensure this revisit frequency.

We use the Earth Engine Code Editor (Google Inc., 2023a) and load SAR data from the Earth Engine Data Catalogue (Google Inc., 2023b) which allows us to perform an online analysis of large data sets, with virtually no computational cost on a desktop computer. Accessing the data as a Level-1 GRD product means that border noise removal, thermal noise removal, radiometric calibration, and terrain correction have already been performed, following pre-processing steps of the Sentinel-1 Toolbox (ESA, 2023d) and leading to a calibrated and orthorectified product with a pixel size of 10×10 m. The ground range detection process projects the slant range coordinates of the radar data represented by range and azimuth onto the ellipsoid of the Earth, resulting in a product which has an approximately square spatial resolution and square pixel spacing (ESA, 2023e). Border noise removal deals with low-intensity noise and invalid data on scene edges. The thermal noise correction removes additive noise in sub-swaths to help reduce discontinuities between sub-swaths for scenes in multi-swath acquisition modes (ESA, 2023f). Radiometric calibration ensures that the intensity value represents the value of the reflectivity, i.e., the radar cross section normalized to the area (Moreira et al., 2013). This backscatter coefficient σ_0 can vary by several orders of magnitude and is therefore converted to decibels, as shown in Eq. (1).

$$\sigma_0 = 10 \log_{10} \sigma_{0\,\mathrm{raw}} \tag{1}$$

It measures whether the radiated terrain preferentially scatters the incident microwave radiation away from the SAR sensor ($\sigma_0 < 0$) or towards the SAR sensor ($\sigma_0 > 0$) (ESA, 2023f). Terrain correction ensures that the location of any pixel in the SAR image is directly associated with the position on the ground. Radar only measures the projection of a three-dimensional scene on the radar coordinates' slant range and azimuth. This causes effects such as shadow for areas hidden from the radar illumination and foreshortening and layover manifested by a stretch and compression of sloped terrain (Moreira et al., 2013). The terrain correction (or orthorectification) is based on the ASTER Global Digital Elevation Model (GDEM) (U.S./Japan ASTER Science Team, 2023), given the high-latitude location of the study area (>60° N) (ESA, 2023f).

2.3 Incoming shortwave radiation and air temperature

We use the current operational version of the Regional Atmospheric Climate Model (RACMO2.3p2), which is a high-resolution regional climate model (RCM) adapted for high latitudes. It has been shown to capture spatial and temporal variability and absolute values well (Noël et al., 2019). Air temperature and shortwave radiation data from

RACMO2.3p2 are used to bring lake-specific climatological variables into context with lake ice break-up timing. We utilize model outputs as opposed to measurements since field observations do not possess the spatial coverage for our large-scale study. The current operational version RACMO2.3p2 is validated against 37 automated weather stations (AWSs) on the GIS and is proven to realistically represent near-surface temperature ($0.73 < R^2 < 0.98$) and cloud conditions through shortwave and longwave radiation components ($0.85 < R^2 < 0.96$). This translates to biases in daily mean air temperatures at 2 m and incoming shortwave radiation of 0.14 °C and 4.8 W m^{-2}, with the latter corresponding to a bias of 2.7 % (Noël et al., 2019).

To estimate excess radiation and energy due to variability in the break-up timing and investigating potential correlations with air temperature, we acquire lake-specific incoming shortwave radiation at the surface and air temperature at 2 m data as climatological daily mean values for the period 1991–2020 from RACMO2.3p2 (Noël et al., 2019). The four nearest grid points of the model from the coordinates of each respective lake center point are selected in order to approximate the radiation and temperature data using Delaunay triangulation (Delaunay, 1934) with cubic interpolation.

3 Methods

3.1 Pre-processing lake inventory and SAR data

We retrieve SAR backscatter data of 14 336 lakes which have a surface area ≥ 0.1 km^2 to exclude potential inaccuracies due to the lake size. Time series of lakes with a temporal resolution below 2 d are excluded from the analysis to produce robust results. While the acquisition frequency varies spatially and might be as high as 1 d, we assume a maximum temporal resolution of 2 d for the entire dataset, which falls short of meeting the daily acquisition criteria of the GCOS ECV lake ice cover for climate monitoring (WMO, 2022b). Backscatter data which lack a pronounced annual evolution and exhibit strong uniform characteristics are also excluded. This means that only lakes with a difference of ≥ 8 dB in mean values of σ_0 between January/February (i.e., most certainly ice-covered) and August/September (i.e., most certainly ice-free) are considered.

3.2 Detecting lake ice break-up from SAR backscatter

The term "lake ice break-up" used in this study describes the timing, i.e., day of year (DOY), when at least 80 % of the lake surface is liquid water and is therefore an approximation to the timing of "water clear of ice" (WCI) (WMO, 2022b). Once snowmelt starts on lake ice, water collects around the margins, where it warms as it absorbs solar radiation and accelerates melting due to positive feedback (Jeffries et al., 2012). We assume that lake ice is present the longest in the central areas of the lake and therefore aim to detect the presence or absence of ice in the central 20 % of the lake surface area, which means that the σ_0 values are averaged for this central portion. This results in an area of approximately 0.02 km^2 for the smallest lake, which corresponds to at least 200 pixels considered for averaging and proves to be a robust measure to identify the phenological state of lake ice.

We apply a locally weighted scatterplot smoothing (LOWESS) filter to attenuate the temporal variability of σ_0 caused by varying incidence angles due to both ascending and descending orbits to ensure a more robust and confident ice break-up detection (Fig. 1a). We found the choice of 1 % of the data for LOWESS filtering to provide robust results for the analysis. For each lake, a dynamic numerical threshold is applied in each year to identify the timing of ice break-up. This yearly threshold amounts to 25 % of the σ_0 difference between the 98th and 2nd percentile and must be at least 2.5 dB. The timing of lake ice break-up is detected when the absolute value of σ_0 decrease exceeds the threshold value within three consecutive acquisitions. Once the break-up timing is identified from the LOWESS data, the DOY of lake ice break-up is assigned to the lowest σ_0 value of the raw backscatter signal within five acquisitions ahead of the detected drop in the LOWESS data (Fig. 1a). The detection algorithm is applied for the period starting from 1 May to exclude early misdetections.

Figure 1a shows a typical SAR backscatter evolution for the period 2017 to 2021 with detected break-up timings. High σ_0 values (e.g., Nov–May) are governed by surface dry conditions of snow and ice (Unterschultz et al., 2009). The first major declines of σ_0 in a given year (e.g., May–June) indicates the onset of melt processes at the surface of the lake ice cover. A smooth, wet ice surface decreases the amount of backscatter due to specular reflection of the radar beam in a direction away from the sensor. A rough, wet ice surface increases the amount of backscatter due to diffuse scattering, reflecting the radar beam nearly uniformly in all directions and directing a proportion of the incident energy back toward the sensor (Unterschultz et al., 2009). The progressing melt on the lake surface leading to a rougher, wetter surface explains the σ_0 recovery before the major backscatter decline in summer that indicates lake ice break-up. We visually inspected time series of Sentinel-2 (S2) imagery for selected lakes to support the observations of the backscatter dynamics and found that this is a typical σ_0 evolution during the period of disintegration which is not related to refreezing processes.

Figure 1a shows that in several years (e.g., from 2017 to 2020) the evolution of σ_0 might be clearly pronounced, while in other years (e.g., 2021) the backscatter decline and identification of the break-up timing is more complex. This is due to the nature of break-up processes being more complex due to melting on top and bottom (Jeffries et al., 2012) or varying acquisition conditions.

Figure 1b shows the results of lake 28 300 in SW Greenland to demonstrate the detection of lake ice break-up in 2019 from SAR data compared to optical satellite imagery from

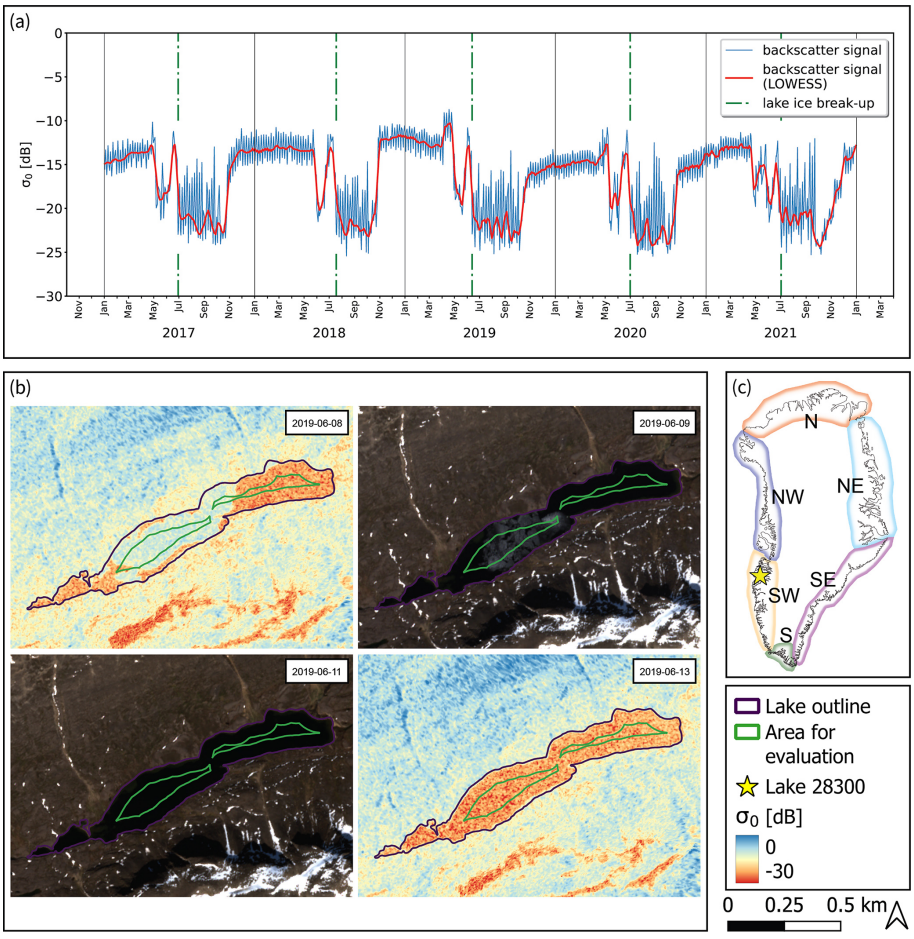

Figure 1. (a) Sentinel-1 (S1) synthetic aperture radar (SAR) backscatter (σ_0) and lake ice break-up timings for lake 28 300 detected from a dynamic numerical threshold assessing the σ_0 decline from being ice-covered to open water. While the LOWESS smoothed backscatter is utilized to confidently identify the period of break-up, the actual break-up timing is derived from the raw backscatter signal. The σ_0 decline and recovery just before the apparent lake ice break-up indicates the onset of snow- and ice melt. **(b)** S1 and Sentinel-2 (S2) images of lake 28 300 during break-up in 2019. The S2 scene shows water clear of ice (WCI) on 11 June 2019, while the break-up timing from S1 is detected on 13 June 2019. **(c)** Regions of Greenland for the spatiotemporal analysis.

the S2 mission. The detection algorithm identifies the lake ice break-up timing on 13 June 2019 from S1 backscatter data, while the S2 image shows water clear of ice on 11 June 2019, which can be taken as the accuracy of the method.

3.3 Analyzing spatial patterns of lake ice break-up timing

The study area is divided into six regions (N, NE, SE, S, SW, and NW) to explore spatiotemporal statistics (Fig. 1c). We chose a significance level of 0.05 to assess differences between regions and years, respectively, and use Pearson correlation coefficient (r) to assess relationships as linear correlations. Furthermore, we group lakes into sections of 1° N latitude and 100 m elevation, respectively, to assess spatial gradients and explore relationships between break-up timing and elevation, between break-up timing and latitude, and between break-up timing and lake surface area. In the result statistics, we include only lakes with detected ice break-up timings in every given year (2017–2021) to get robust detection statistics and to mitigate random detections. Furthermore, we manually remove obvious misdetections after visual inspection of the backscatter time series, since we prioritize robust results statistics over a fully automatically detected larger sample size that includes misdetections.

3.4 Assessing climatological variables in terms of lake ice break-up timing

3.4.1 Calculating cumulative positive degree days

In order to understand the relationship between the annual evolution of air temperature, incoming radiation, and median lake ice break-up timings, we calculate the climatological mean of positive degree days (PDDs) from RACMO2.3p2 2 m daily air temperature averages for the period 1991 to

2020 and analyze them as cumulative values from 1 January until the median DOY of break-up. With this we support our discussion on the complexity regarding determining factors such as latitude, elevation, and radiation in the context of cumulative PDDs.

3.4.2 Calculating excess radiation and energy

In order to determine the impact of varying lake ice cover on the radiation and hence the energy balance, we acknowledge several factors. (I) The surface albedo of the lake surface changes rather abruptly from ice to open water. In that way, the same radiation and energy input gets converted to drastically higher energy amounts at the surface after ice break-up. (II) Depending on what time of the year the break-up happens, one will have a different impact on the energy balance. To illustrate the different impact a given change in lake ice break-up may have, we assume three arbitrary lakes of the same size at the same latitude (and hence with the same arbitrary potential incoming shortwave radiation values) and show the impact in a conceptual way in Fig. 2. Assume that, for instance, due to elevation differences, lake A typically breaks up some weeks before, lake B at the time of incoming radiation maximum, and lake C some weeks afterwards. If we now assume changing conditions in a way that all three lakes break up 8 d (which corresponds to the median MAD and is described in Eq. 4) earlier than under "regular" conditions, we see the following. For lake A, less energy gets added, since it is at a time when radiation input is comparably low, while lake B changes the energy input more strongly. For lake C, it means that despite having the same temporal distance between the break-up timing and the radiation maximum as lake A, the excess radiation and energy input become higher since the period falls into a time with high incoming radiation. We coin the terms "excess radiation (input)" and "excess energy (input)" to describe the additional added radiation and energy due to an earlier lake ice break-up timing of 8 d compared to the observed median timings between 2017 and 2021 for each respective lake. (III) The lake size plays a role in the total budget considerations. Large lakes have larger surface areas over which the energy can be accumulated. (IV) Finally, the shortwave radiation input is determined by latitude and altered by regional effects (e.g., cloud cover) or local effects (e.g., shading due to geometry) which are accounted for in the RACMO2.3p2 data (Noël et al., 2019).

We quantify the excess radiation input H_{SW} ($J\,m^{-2}$) for each lake as a consequence of an earlier break-up by integrating the shortwave radiation balance (incoming radiation G ($W\,m^{-2}$) minus the reflected shortwave incoming radiation R ($W\,m^{-2}$)) between 8 d before DOY_m and the median lake ice break-up timing DOY_m, as shown in Eq. (2).

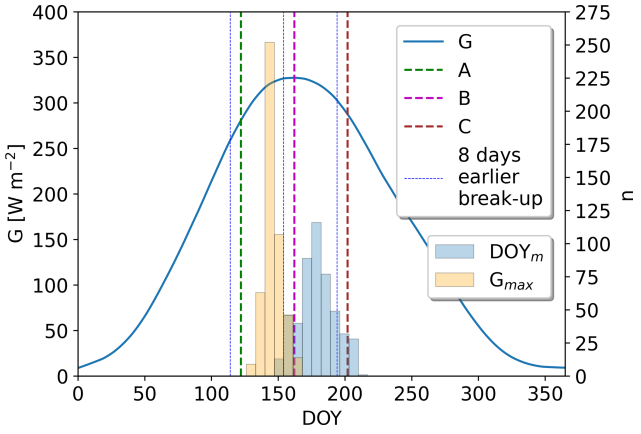

Figure 2. Conceptual lake ice break-up timings of three arbitrary lakes (A, B, and C), histograms of lake-specific median lake ice break-up DOY_m, and timing of maximum incoming radiation G_{max}. Assuming that all three lakes break up a fixed number of days earlier than their median break-up timings (in this case 8 d earlier, which is the median variability in our data), it can be hypothesized that when considering the annual evolution of global radiation G at the surface, lake A receives less additional energy, lake B at the solar radiation maximum the most energy, and lake C comparably higher additional energy than lake A. The median day of year (DOY) of DOY_m and G_{max} in our data are 178 and 145, respectively, indicating that most of the lakes will correspond to lake C.

$$H_{SW} = \int_{DOY_{m-MAD}}^{DOY_m} G(t) - R(t)\,dt \quad (2)$$

The reflected shortwave incoming radiation R ($W\,m^{-2}$) is calculated from the albedo difference $\Delta\alpha$ between the assumed values of snow-covered lake ice α_i (0.9) and open-water α_w (0.1), as shown in Eq. (3).

$$R = G\,\Delta\alpha \quad \text{with} \quad \Delta\alpha = \alpha_i - \alpha_w = 0.8 \quad (3)$$

We hypothesize that an earlier lake ice break-up impacts the timing of the entire lake ice disintegration process from the melting of the initially dry snow cover on top of the lake ice until the melting of the bare ice surface itself. The short-term albedo development might be highly variable, impacting the transition from dry to wet snow, from wet snow to bare ice, and from bare ice to open water. We assume that the earlier break-up exhibits a shift in the entire disintegration period while its length is maintained, which means that the period of the snow-covered lake is 8 d shorter, while the period of the lake having an open-water surface is 8 d longer. Therefore, the albedo difference $\Delta\alpha$ is expressed as the change from snow-covered lake ice α_i (0.9) to open-water α_w (0.1) to quantify the excess radiation input H_{SW}.

The chosen 8 d for the hypothesized earlier lake ice break-up correspond to the median of the lake-specific median absolute deviation (MAD) describing the variability in the an-

nual break-up timings DOY_i around the median DOY_m of this period, as shown in Eq. (4),

$$\begin{aligned} \mathrm{MAD} &= \mathrm{median}\left(|\mathrm{DOY_i} - \mathrm{DOY_m}|\right) \\ &\text{with} \quad \mathrm{DOY_m} = \mathrm{median}\left(\mathrm{DOY_i}\right), \end{aligned} \tag{4}$$

where DOY_i stands for the break-up timing in each respective year from 2017 to 2021. This can be regarded as a realistic period for an assumed earlier deviation of the break-up timings of all lakes to assess the impact of varying lake ice cover on the radiation balance.

Furthermore, we calculate the excess energy input E_{SW} (J) for each lake by multiplying the excess radiation H_{SW} ($J\,m^{-2}$) for the 8 d earlier lake ice break-up with the respective lake areas A_i (m^2), as shown in Eq. (5).

$$E_{SW} = H_{SW}\, A_i \tag{5}$$

In that way, we consider general radiation conditions, lake size, and albedo change and express its reaction on a change in timing. Clearly, a change in the break-up timing at or just after the radiation maximum of a large lake will have a higher impact than a change later in the season for a small lake.

In order to make the results more tangible, we calculate what the excess energy inputs E_{SW} mean in terms of mass and volume ice melt at the melting point (m_i, V_i) and water temperature increase (m_w, V_w). For this reason, we convert the summed energy input E_{SW} of all lakes using the latent heat of fusion L_f ($334\,000\,J\,kg^{-1}$), the specific heat capacity of water c_w ($4184\,J\,kg^{-1}K^{-1}$), and the assumed densities of ice at the melting point ρ_i ($999\,kg\,m^{-3}$) and water close to freezing point ρ_w ($999\,kg\,m^{-3}$), as shown in Eqs. (6) and (7).

$$m_i = \frac{\Sigma E_{SW}}{L_f} \quad \text{and} \quad V_i = \frac{m_i}{\rho_i} \tag{6}$$

$$m_w = \frac{\Sigma E_{SW}}{c_w} \quad \text{and} \quad V_w = \frac{m_w}{\rho_w} \tag{7}$$

Our calculations show that lake surface area A_i strongly determines the excess energy input E_{SW} and explains more than 99 % of its variability in the dataset (Fig. D2). This allows translating the excess energy input E_{SW} to the ice thickness melted or water depth warmed by 1 K across the respective lake surface area which are derived the from excess radiation input H_{SW}. For this estimate, we ignore lake bathymetry and present the mean values of melted thickness of ice at the melting point h_i (m) and depth of water h_w (m) warmed by 1 K, as shown in Eqs. (8) and (9).

$$h_i = \mathrm{mean}\left(\frac{H_{SW}}{L_f\,\rho_i}\right) \tag{8}$$

$$h_w = \mathrm{mean}\left(\frac{H_{SW}}{c_w\,\rho_w}\right) \tag{9}$$

3.5 Validating detected lake ice break-up timings

The break-up detection is assessed and validated in three ways. (I) We utilize daily time-lapse images of three lakes (Badesø, Langesø, and Quassi-sø) in vicinity of Kobbefjord (SW Greenland) between 2017 and 2020 (Abermann et al., 2019) to quantify the mean error of lake ice break-up of those lakes compared to the detection algorithm. (II) We use lake ice break-up data from observations, thermistor data, and satellite imagery in the Kangerlussuaq area (SW Greenland) between 2017 and 2021 (Saros et al., 2019). While there are no corresponding lakes from the validation data included in our study due to a lack of pronounced radiometric properties, we compare median lake ice break-up timings between 11 lakes used for validation and 14 lakes in our study in vicinity to each other. (III) We access daily data from ESA CCI (ESA, 2023a) for "lake ice cover (LIC)" to validate the break-up timing of two lakes (SW Greenland). These data are generated from MODIS imagery from both the Terra and Aqua satellite missions.

4 Results

4.1 Lakes and regions suitable for lake ice break-up detection and analysis

We restrict our analyses to the S, SW, and NW regions, since a comprehensive analysis for lakes in the N, NE, and SE is not possible due to challenging radiometric characteristics and/or temporal resolution (Tables A1 and A2), leaving a sample size that is too small. Since we only consider lakes with detected break-up timings in every given year between 2017 and 2021 and remove obvious outliers manually, we end up analyzing 563 lakes, which are 21 lakes in S, 450 lakes in SW, and 92 lakes in NW. This corresponds to 0.4 % of all lakes or 6.8 % of the overall lake area in the inventory. The data coverage of RACMO2.3p2, however, allows analyzing 491 lakes, which include 21 lakes in S, 406 lakes in SW, and 64 lakes in NW, with regard to excess radiation and energy inputs and cumulative PDDs. This represents 0.3 % of all lakes or 6.8 % of the overall lake area in the inventory (Tables A1 and A2).

4.2 Lake ice break-up detection validation

The detection of the lake ice break-up timings from SAR data proves to be conservative (i.e., later) compared to the lakes from all three validation approaches and allows characterizing the break-up timing with a mean error of 5 d at maximum. Yearly mean errors in the three compared lakes validated from time-lapse cameras range from 1–18 d, exhibiting an overall mean error of 5 d (Table B1). Yearly differences between the median break-up timings of 14 lakes compared to 11 surrounding lakes used for validation in the Kangerlussuaq area range from 3–7 d, with an overall difference of 5 d, indicating that the interannual variability is well captured (Table B2). The two lakes validated from the ESA CCI data yield yearly mean errors ranging from 0–5 d with an overall mean error of 2 d (Table B3).

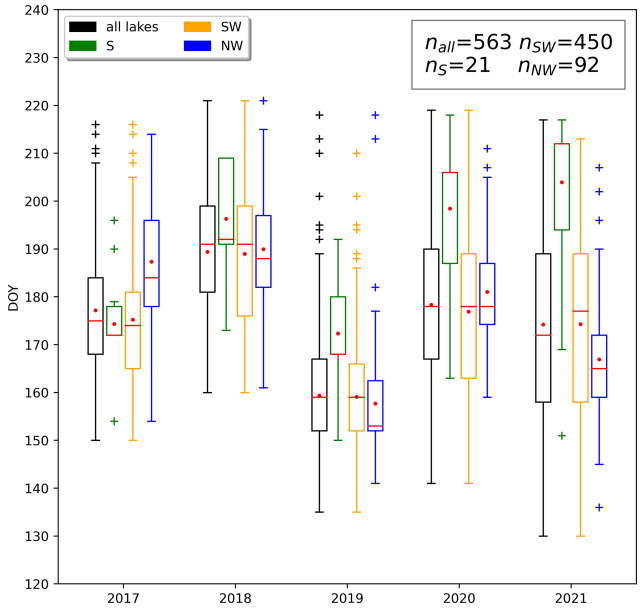

Figure 3. Lake ice break-up timings of all studied lakes and grouped by region. Red lines indicate median values, while red dots represent mean values. Median break-up timings are earliest in 2019 (8 June) and latest in 2018 (20 July). Lakes in the S region break up significantly later in 2018–2021 compared to the other regions, while lakes in NW tend to break up earliest. This can be attributed to mainly higher-elevated lakes in S and mainly lakes close to sea level in NW.

4.3 Lake ice break-up timing across S, SW, and NW Greenland and elevation gradients

Median break-up DOY of all lakes range between 159 in 2019 and 191 in 2018, which corresponds to dates between 8 June and 10 July (Fig. 3). Regional annual median DOY range from 168–212 (S), from 159–191 (SW), and from 153–188 (NW). Annual lake ice break-up DOY in S are significantly later for 2018 to 2021 compared to SW and NW. In 2017, the median break-up DOY in S exhibits no difference to SW and is significantly earlier compared to NW. The annual break-up timings in SW are significantly earlier in 2017 and significantly later in 2021 compared to NW.

Lake-specific break-up timings, as well as median break-up DOY for 2017 to 2021, increase with elevation (Fig. 4a), while no confident latitudinal gradients or correlations with lake surface area could be identified (Fig. 4b; Table C1). Median break-up DOY for the period 2017 to 2021 increase by 3 d per 100 m elevation gain ($r = 0.76$; $p<0.01$) (Fig. 4a), while yearly lake ice break-up DOY show strong correlations ($0.51 \leq r \leq 0.78$; $p<0.01$) with elevation, exhibiting increases of 2–4 d per 100 m (Fig. C1). For a given elevation band, we find that lake ice in more northern latitudes tends to break-up later but exhibits only weak correlations (Table C1).

Subdivided into latitudinal bands of 1° between 60 and 71° N, strong correlations (up to $r = 0.89$; $p<0.01$) between break-up timing and elevation can be identified in several years. Those exhibit an increase of 3–6 d per 100 m, depending on the latitudinal band, as well as the elevation range, and are significant in 43 out of the 55 yearly correlations (Figs. C2–C5). The median break-up dates for the period 2017 to 2021, except between 60–61 and 70–71° N, show strong correlations ($0.64 \leq r \leq 0.85$; $p \leq 0.01$) increasing by 3–6 d per 100 m elevation increase.

4.4 Lake ice break-up timing compared to cumulative PDDs until lake ice break-up

Figure 5 shows an increase in cumulative PDDs until lake ice break-up with increasing median break-up DOY. A later break-up timing at lower latitudes can be observed in Fig. 5a when comparing lakes in a similar cumulative PDD range. Figure 5b shows that lakes with similar cumulative PDDs experience a later lake ice break-up at higher elevation. This is due to mainly higher-elevated lakes at lower latitudes as opposed to lower-elevated lakes at higher latitudes. Comparing two lakes at different elevations with a similar break-up timing, we see that a higher-elevated lake with lower cumulative PDD values needs a comparably higher energy input (or lower energy output) to accommodate the same break-up timing as the lower-elevated lake with comparably higher cumulative PDDs. This is provided by a location at lower latitudes with comparably more incoming shortwave radiation.

4.5 Excess radiation and energy from earlier lake ice break-up

Referring to the concept shown in Fig. 2, which describes the median lake ice break-up timings in relation to the timing of maximum incoming solar radiation, we find that virtually no lakes represent case A (<0.01 %), approximately 5 % represent case B, which is around the respective radiation maximum (±8 d), while case C applies to approximately 95 %. The median time difference between the lake-specific maximum incoming radiation and median break-up amounts to 35 d (Fig. D1). Figure D1 shows that excess radiation H_{SW} is highest for lakes around and after the radiation maximum, while H_{SW} values are decreasing with the increasing later timing of the median break-up (i.e., increasing distance from the solar radiation maximum). The highest H_{SW} values can be found at low latitudes and at high-latitude lakes at lower elevation (Fig. 6). At lakes with similar latitudes, higher H_{SW} values are found at lower elevations, while at lakes with similar elevations, excess radiation values are typically higher at lower latitude.

Figure 7 shows the lake-specific results for E_{SW} as a function of latitude (Fig. 7a) and elevation (Fig. 7b). We clearly find larger E_{SW} values for larger lakes and a weaker, yet visible, dependence with latitude. Regarding a relation to elevation, we see generally larger E_{SW} for lower elevations, which is partly due to the fact that larger lakes typically develop

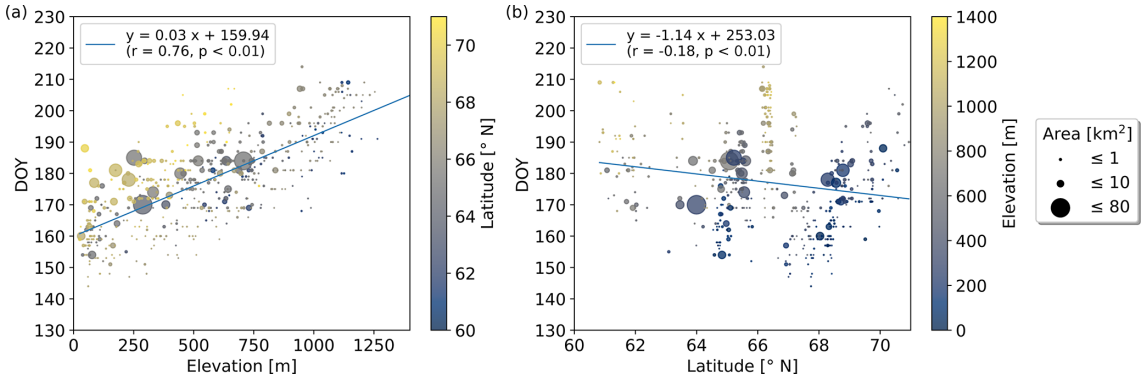

Figure 4. Median break-up timings DOY_m for the period 2017 to 2021 vs. **(a)** elevation and **(b)** latitude. DOY_m increase by 3 d per 100 m elevation gain exhibiting a strong correlation ($r = 0.76$; $p<0.01$) while only a weak correlation with latitude can be identified.

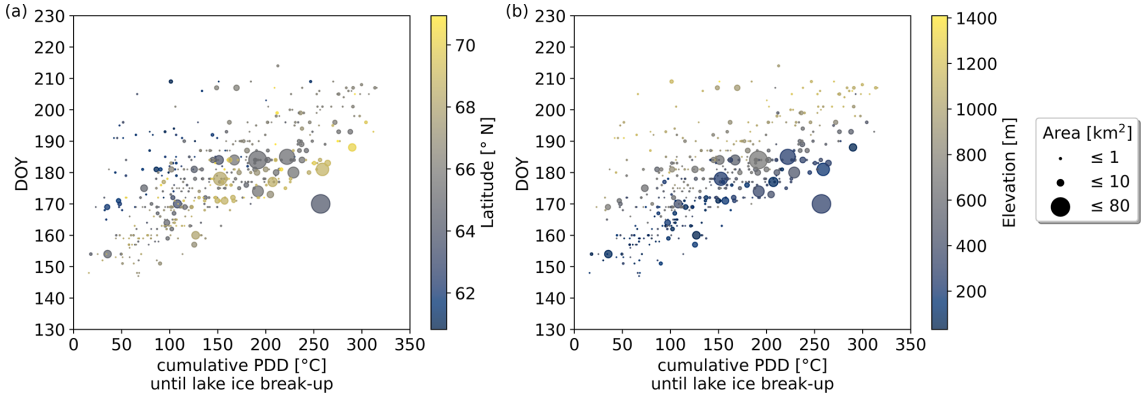

Figure 5. Median break-up timings of the DOY_m for the period 2017 to 2021 vs. cumulative positive degree days (PDD) until lake ice break-up, with color signatures for **(a)** latitude and **(b)** elevation. The influence of air temperature and radiation on the break-up timing (i.e., in the energy budget) can be assessed when comparing two lakes at different elevation with a similar break-up timing. While the lower-elevated lake has higher cumulative PDD values and is located at higher latitude, the higher-elevated lake with lower cumulative PDDs is located further south.

in lower elevations. Also, the fact that high-elevated lakes typically break up later after the radiation maximum plays a role in that regard. We find that the summed excess energy of all 491 analyzed lakes, which amounts to 133 250 TJ, corresponds to melting 0.4 Gt ice or an ice cube of 7.4 km length. Likewise, the same energy input could heat up 31.9 Gt water or a water cube of 31.7 km length by 1 K.

Our calculations on excess energy show that lake surface area strongly determines the added energy and explains more than 99 % of its variability in the dataset (Fig. D2). When referring the added energy in terms of ice melt and water temperature rise to the lake-specific areas in a simplified way which ignores lake bathymetry, we find that the excess energy input averagely corresponds to melting 0.4 ± 0.1 m thick ice or heating up a water depth down to 35 ± 3 m by 1 K across the entire surface area. If we upscale our results to all 100 486 lakes in S, SW, and NW (<71° N) Greenland based on the strong relationship between excess energy and surface area while assuming similar radiation conditions and lake ice break-up variabilities, we estimate an additional energy input of 1.8×10^6 TJ, which corresponds to melting 5.8 Gt ice at the melting point or warming 432.3 Gt water by 1 K. The number of lakes corresponds to 64.5 % of all lakes or 62.1 % of the overall lake area in the inventory (Tables A1 and A2). To put this into perspective, the upscaled mass estimate of ice melt corresponds to approximately 30 % to 60 % of the volume of Greenland peripheral glaciers published in recent studies (Hock et al., 2023).

5 Discussion

5.1 Limitations and potential

In our study, we apply a dynamic numerical threshold on the annual SAR backscatter evolution to establish an automated detection of lake ice break-up timing. Differences in the dielectric properties between water and ice which are manifested in a decline in the radar backscatter (Unterschultz et

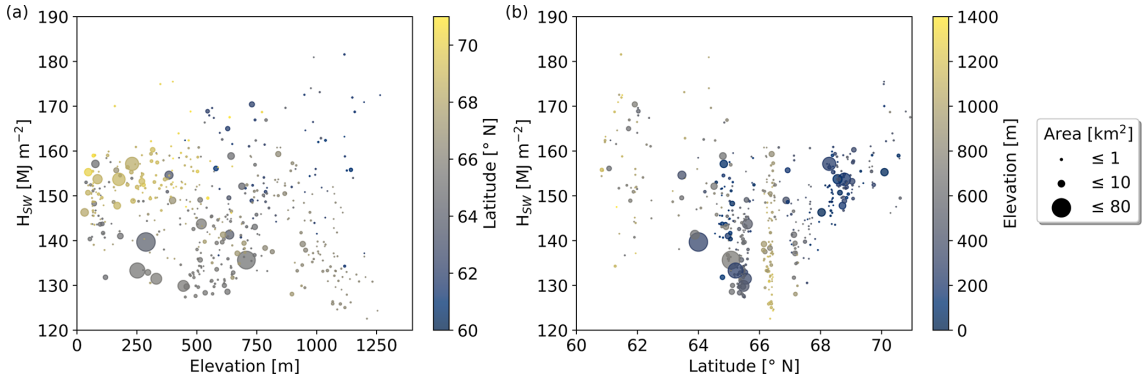

Figure 6. Excess radiation H_{SW} due to lake-specific break-up timings which are 8 d earlier compared to the median break-up timings for the period 2017 to 2021 vs. **(a)** elevation and **(b)** latitude. High H_{SW} values are found for lakes at low latitudes and at high latitudes with low elevation.

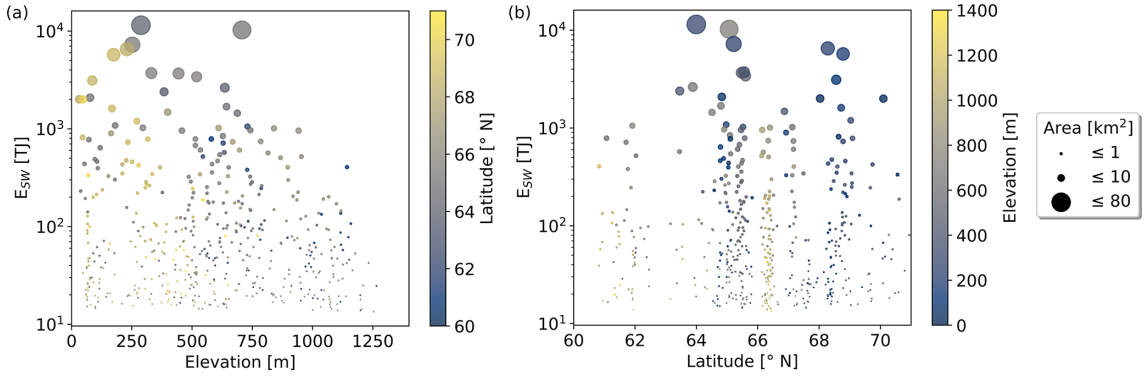

Figure 7. Excess energy E_{SW} due to lake-specific break-up timings which are 8 d earlier compared to the median break-up timings for the period 2017 to 2021 vs. **(a)** elevation and **(b)** latitude. Lake surface area strongly determines the excess energy. The largest E_{SW} are found at mid-latitudes and low elevation, since larger lakes typically developed there.

al., 2009) and the fast transition from an ice-covered to an open-water surface allow for an automated detection. In contrast, different modes of lake surface freeze-up, and high local and interannual variability in the backscatter during long periods of gradual freezing makes an automated detection of the freeze-up very challenging. This limitation in the automated detection method constrains this study to an analysis of the variability in lake ice break-up timing as opposed to an analysis of spatial and temporal variations in the length of the period in which the lake surface is frozen. However, we argue that regarding the impact of lake ice presence on surface energy balance, the break-up timing of lake ice is more relevant than the timing of the freeze-up. In our data, we see that freeze-up typically occurs in October or November when incoming solar radiation is lower than during the timing of break-up (yearly median break-up timings vary between 8 June and 10 July) (Fig. 2).

Our presented vertical gradients of break-up timings on the order of a few days must be interpreted with regard to the temporal limitation of the data and method. The SAR data with an acquisition resolution of 2 d implies a maximum accuracy of ±1 d for detecting lake ice break-up, while the validation indicates that our automated detection exhibits a mean error of 2–5 d. The GCOS ECV requirements state that the temporal resolution of our study allows for contrasting extreme ice years, numerical weather forecasting, and assessing lake models (WMO, 2022b). In a related study, Murfitt and Duguay (2020) also utilized S1 high-density time series data to monitor ice phenology of Lake Hazen located in Nunavut, Canada (81.78° N, 71.05° W). They found mean errors of 3–7 d for comparing sectional WCI dates and 3–5 d for a pixel-based ice-off comparison, which is in agreement and of the order of our validation results.

The estimates of the excess radiation and consequently excess energy are based on assuming a shift in the entire break-up process while having its length maintained. This means that the excess energy is assumed to be available for the open-water surface of the lake and is not utilized during the break-up process. Short-time albedo development during the disintegration process of the lake surface might be highly variable, and changes in the configurations and lengths of the transition from dry to wet snow, from wet snow to bare ice,

and from bare ice to open water might vary greatly with elevation, latitude, and local climates. A site-specific characterization of albedo evolution during lake ice break-up might be a subject for further studies and improve local excess energy estimates.

5.2 Lake ice break-up in context of coastal climate and topography

We assess that elevation more strongly determines the lake ice break-up timing in Greenland than latitude does. For all lakes and lakes grouped by latitudinal sections, we demonstrated that there are strong correlations between median break-up timings and elevation, as well as yearly break-up timings and elevation. The significantly later timing of the yearly median break-up DOY in S compared to SW and NW across several years can be explained by the hypsometry of the terrain and the distribution of lakes with elevation (fewer lakes close to sea level). Local topography and the extent of fjord systems can have a strong influence on the timing of ice break-up, which may be due to local climate influences and sea ice. This is demonstrated by lakes with early break-up timings in close vicinity to fjords such as between 67.5 and 68.5° N (Fig. 8a, orange arrow) as opposed to lakes with late break-up timings at high-elevation areas (>1000 m) being surrounded by ice bodies such as between 66.0 and 66.5° N (Fig. 8a, blue arrow). When discussing break-up timing in context of topography, the spatial distribution of snowfall must also be considered. The amount of snowfall may greatly influence the variability in the lake ice due to its insulating properties on top of the lake ice surface, as well its role during lake ice build-up and disintegration. The difference in break-up timing between coastal lakes, which is earlier at 67.5–68.5° N compared to being later at >68.5° N may be attributed to higher snow accumulation rates which can be as much as 3 times higher in the latter case, as shown by Bales et al. (2009).

Imrit and Sharma (2021) found that climate change, warmer local air temperatures, and teleconnection patterns are able to explain on average approximately 60 % of the variation in ice phenology of lakes in North America and Europe. On average, approximately 40% of the variation remained unexplained and could be attributed to local weather conditions, such as solar radiation inputs, wind, snow cover, and lake and landscape characteristics, such as lake depth, elevation, and fetch. This is in line with our interpretation of variability in the timing of lake ice break-up which may be greatly attributed to local weather, climate, and landscape characteristics in coastal Greenland.

Lake ice break-up timings of the years 2018 (Fig. 8b) and 2019 (Fig. 8c) which exhibit the latest (DOY 191; 10 July) and earliest (DOY 159; 8 June) median lake ice break-up DOY within the observed period are in line with temperature observations. Mean summer and July temperatures in 2019 were among the 6 warmest years (1981–2019), while comparably cooler June–August (JJA) air temperatures at Greenland coastal stations were recorded in 2018 (Hanna et al., 2021).

5.3 Lake ice break-up in Greenland compared to other study sites

L'Abée-Lund et al. (2021) studied the phenology of 101 Norwegian lakes between 1890–2020, covering a latitudinal range of 58.2–69.9° N, and found stronger correlations between the average timing of ice break-up and elevation (3.4 d per 100 m; $r = 0.63$; $p<0.01$) when compared to the correlations between break-up timing with latitude (2.3 d per 1° N; $r = 0.35$; $p<0.01$.). Williams et al. (2004) and Williams and Stefan (2006) assessed lake ice break-up timing of approximately 140 lakes in North America (between 40.0 and 82.5° N) from records between 1848 and 1997 and found that there is a strong relationship between break-up timing and latitude, arguing that geographic latitude is a good indicator of climate. They showed that only a weak relationship between elevation and the timing of break-up was observed when grouping the data by region, presenting an increase in the break-up timing of 2 d per 100 m elevation increase. Zhang et al. (2021) found a strong correlation between latitude and lake ice-break up timing ($R^2 = 0.75$) and only a weak relationship with elevation for 4241 lakes in Alaska over the period 2000–2019.

In our study, which covers lakes between 60 and 71° N, however, we find strong correlations between break-up timing and elevation and only a weak relationship with latitude for lakes at similar elevation. This again highlights the influence of the spatial configuration of lakes in Greenland determined by the proximity to both the ocean and the GIS, the presence of fjord systems and the steep slopes.

5.4 Lake ice break-up and climate change

Magnusson et al. (2000) found that lake ice break-up dates in the Northern Hemisphere from 1846 to 1995 became on average 6.5 d earlier per century, corresponding to an air temperature increase of approximately 1.2 °C during this period. They claim that the interannual variability in the break-up timing increased since 1950. Hallerbäck et al. (2022) studied lake ice phenology in Sweden from observations spanning the period 1700–2014 and found that the break-up timing of northern lakes (>60° N) advances by 4.4 d per 1 °C of warming. Our observed variability of ±8 d based on the period 2017–2021 lies above the observed break-up shift over 100 years, which might be attributed either to the increased variability in recent years or to the exceptional years 2018 and 2019 greatly skewing the variability in the short observational period. Imrit and Sharma (2021) showed that 18 lakes around North America and Europe were thawing 9 d earlier per century over the past 156–204 years. They argued that by adding 24 years of data to the previous study of Magnusson

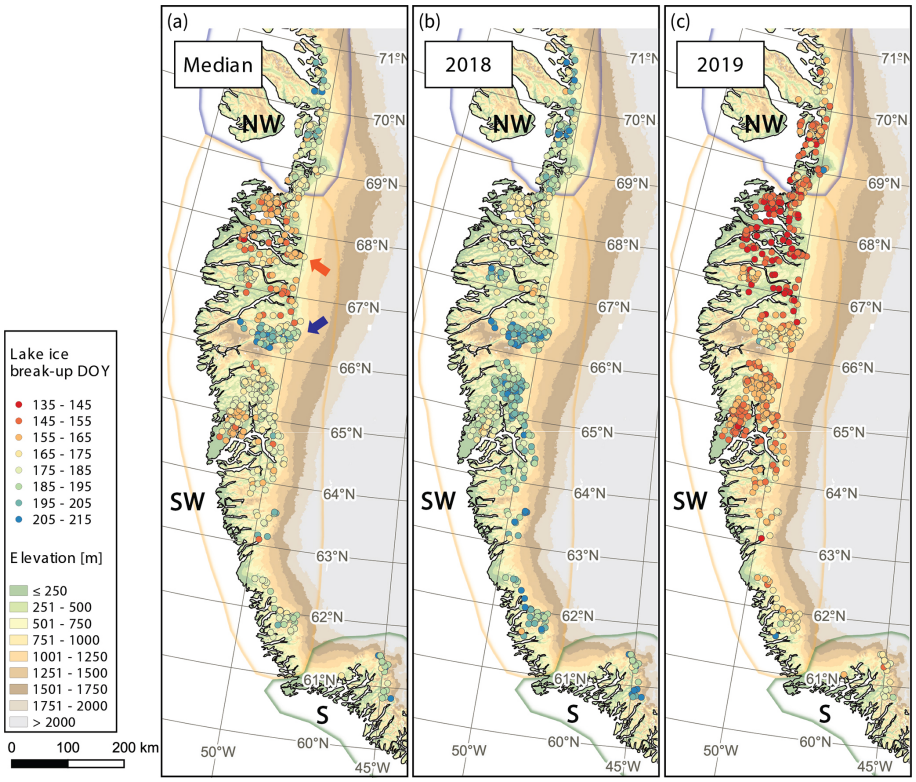

Figure 8. **(a)** Median lake-specific break-up timings for the period 2017 to 2021 and break-up timings for **(b)** 2018 and **(c)** 2019. Local topography such as higher elevation (blue arrow) and extent of fjord systems (orange arrow) can strongly influence lake ice break-up dates. The year 2018 exhibits the latest break-up timings, while the year 2019 shows the earliest break-ups in our studied period, corresponding to median dates 10 July (DOY 191) and 8 June (DOY 159), respectively.

et al. (2000), rates of lake ice loss are almost 1.5 times faster, which may be attributed to warmer air temperatures and a higher prevalence of extreme events in recent decades.

Increased rainfall and especially a prolonged rainfall period may have indirect effects on the lake ice break-up timing due to snowpack heating through percolation and refreeze and a subsequent melt–albedo feedback initiated by heat and rainfall (Box et al., 2022; Box et al., 2023). Projections of temperature increase in the range of 1.5–5.0 °C until 2100, and a trend of precipitation change from snowfall to rainfall (IPCC, 2023) may result in an earlier break-up timing of lakes in Greenland and an increased variability until the end of this century. Using a one-dimensional thermodynamic model for simulating lake ice conditions for 471 lakes in the Northern Hemisphere, Huang et al. (2022) estimated that the global mean lake-area-averaged ice break-up date is projected to advance by 20 ± 7 d over 2020–2100, which translates to an average ice duration decrease by 9.9 d for a 1 °C warming. They claim that the lake ice break-up timing in the Canadian Arctic, northern Siberia, and close to the Barents Sea can be clearly linked to the enhanced polar warming over sea ice areas in the Arctic Ocean in the cold season. They hypothesize that the opening of sea ice in summertime leads to the absorption of anomalous heat by the ocean. In wintertime, the excess heat can reduce sea ice coverage, which in turn generates large heat fluxes from the warmer ocean to the highly stratified winter atmosphere. The atmospheric heating spreads further to neighboring land areas, where it can influence lake ice. Furthermore, Huang et al. (2022) discussed the ice–albedo feedback on lake ice. Due to future ice loss and reduced surface albedo, lakes will absorb more shortwave radiation in the extended ice-free season. The excess heat can reduce ice cover in winter, therefore leading to earlier ice break-up, which in turn triggers a positive feedback in spring.

5.5 Implications of lake ice break-up variability

The magnitudes of our estimated excess energies from earlier break-up timings indicate potentially vast changes in the energy balance with increasingly earlier break-up dates and increasing variabilities due to a changing climate. Furthermore, changes in lake ice phenology which influence subsurface mixing, temperature, and light conditions have a direct impact on the ecosystem. These ramifications due to an earlier lake ice break-up timing may manifest themselves in increases in hypolimnetic oxygen concentrations because of changes in the lake mixing regime, potential earlier and

more CO_2 emissions by lakes during lake ice melting, earlier thermal stratification, a longer open-water season for warming, higher water temperatures, increased evaporation rates, and potentially decreasing water levels. Furthermore, shifts in phytoplankton biomass, food web dynamics, and community composition may occur due to unpredictable changes in lake mixing regimes (Imrit and Sharma, 2021). Below-ice aquatic biodiversity is often tied to the presence of ice, which in turn impacts the seasonal cycle of prey and predators, nutrient cycling, dissolved oxygen, and the timing of algal blooms which may impact ecological processes even in summertime (Huang et al., 2022). Lake ice break-up timing may also have further downstream implications, such as freshwater input into fjords with regard to the transport of nutrients and sediments which influence the geochemical composition and ultimately the marine primary production (Abermann et al., 2021).

Besides these direct impacts in natural systems, the variability in lake ice break-up exhibits several anthropogenic implications. Climate change is likely influencing the thickness of lake ice, as well as the timing of breakup, which has a significant impact on both reservoir inflows and outflows for hydropower (Cherry et al., 2017), as well as on its infrastructure such as damns, spillways, channels, reservoirs, tunnels, inlets, and outlets (Gebre et al., 2013). Changes in phenological ice regimes will make access to lakes more uncertain and potentially hazardous and may impact traditional subsistence-based lifestyles which are dependent on the natural network for access to isolated communities, remote industrial developments, hunting, fishing, herding, and trapping areas (Prowse et al., 2011).

6 Conclusion

We demonstrated that temporal high-resolution S1 SAR data can be utilized to detect lake ice break-up timings in SE, S, SW, and NW Greenland. Our presented lake ice break-up timing results prove to be robust and conservative (i.e., later), with a mean error of maximum 5 d, and allow for a spatiotemporal characterization. We show that median lake ice break-up timings for the period 2017 to 2021 increase by 3 d per 100 m elevation increase, while no strong correlations can be found regarding latitude or lake area.

The 491 studied lakes exhibit a typical variability in break-up timing of ± 8 d. When we assume the break-up timing to be 8 d earlier for each lake, the introduced excess energy corresponds to melting 0.5 m thick ice at the melting point or heating up a water depth down to 35 m by 1 K across the respective surface areas. Scaling up our results to 100 486 lakes across S, SW, and NW Greenland, the excess energy input amounts to approximately 1.8×10^6 TJ for the hypothesized earlier lake ice break-up. The variability in lake ice break-up timing of the studied lakes in Greenland for 2017–2021 is above the observed variability in the related lake ice phenology studies in other regions over the last century which may be attributed to exceptional temperature years in recent years and the comparable short study period. However, with progressing climate change, an increased interannual variability and earlier timing in lake ice break-up can be expected.

Excluding data from days with high wind speeds or coupling the SAR-based detection with optical detections from satellite systems (e.g., S2) might yield more robust results with a higher accuracy but might also decrease the temporal resolution. Applying machine learning or deep learning algorithms as a next step might further improve the break-up detection and increase the sample size. There is the potential to explore the relationship between break-up timing and climatological variables and assess the impact on the energy budget in greater detail by incorporating a variety of parameters into more complex models. Coupling satellite-derived break-up results with a greater number of ground observations and in situ measurements of meteorological variables might further improve remotely sensed break-up detections. A continued study of lake ice break-up timings detected from spatial and temporal high-resolution SAR data such as from S1 will be of high importance in terms of climate monitoring with more data available from increasing operational periods. We aim at applying our algorithm to an analysis of lake ice break-up timing on a global scale.

Appendix A

Table A1. Number of lakes through the different analysis steps in our study, as well as their relative coverage, compared to the entire lake inventory. We found that only lakes in S, SW, and NW Greenland are suitable to perform a spatiotemporal analysis of break-up timings and a statistical analysis considering climatological data.

		Inventory	$A_i \geq 0.1\,km^2$	After pre-processing[1]	With all DOY detected	After outlier removal[2]	With climate data[3]	Upscaled excess energy[4]
All lakes		155 870	14 336	1693	828	563	491	100 486
N		18 631	1613	4	3	0	0	0
NE		19 363	1973	1	1	0	0	0
SE	Abs.	8402	547	2	0	0	0	0
S		11 301	792	54	33	21	21	11 301
SW		79 147	7667	1360	640	450	406	79 147
NW		19 013	1741	272	151	92	64	10 024
All lakes		100.0 %	10.0 %	1.1 %	0.5 %	0.4 %	0.3 %	64.5 %
N		12.0 %	1.0 %	<0.1 %	<0.1 %	0.0 %	0.0 %	0.0 %
NE		12.4 %	1.3 %	<0.1 %	<0.1 %	0.0 %	0.0 %	0.0 %
SE	Rel.	5.4 %	0.4 %	<0.1 %	0.0 %	0.0 %	0.0 %	0.0 %
S		7.3 %	0.5 %	<0.1 %	<0.1 %	<0.1 %	<0.1 %	7.3 %
SW		50.8 %	4.9 %	0.9 %	0.4 %	0.3 %	0.3 %	50.8 %
NW		12.2 %	1.1 %	0.2 %	0.1 %	0.1 %	0.0 %	6.4 %

[1] Lakes with suitable temporal and radiometric characteristics for the automated lake ice break-up detection algorithm. [2] Lakes used for spatiotemporal analysis. [3] Lakes used for analysis of excess radiation, energy, and cumulative PDDs. [4] Lakes used for the upscaled results of excess energy.

Table A2. Surface area (km^2) of lakes through the different analysis steps in our study, as well as their relative coverage, compared to the entire lake inventory. We found that only lakes in S, SW, and NW Greenland are suitable to perform a spatiotemporal analysis of break-up timings and a statistical analysis considering climatological data.

		Inventory	$A_i \geq 0.1\,km^2$	After pre-processing[1]	With all DOY detected	After outlier removal[2]	With climate data[3]	Upscaled excess energy[4]
All lakes		14 183	11 879	2770	1485	971	925	8806
N		2165	1876	12	12	0	0	0
NE		2198	1896	36	36	0	0	0
SE	Abs.	372	260	11	0	0	0	0
S		570	416	29	18	15	15	570
SW		7381	6214	2310	1148	810	788	7380
NW		1497	1217	372	271	146	122	854
All lakes		100.0 %	83.8 %	19.5 %	10.5 %	6.8 %	6.5 %	62.1 %
N		15.3 %	13.2 %	0.1 %	0.1 %	0.0 %	0.0 %	0.0 %
NE		15.5 %	13.4 %	0.3 %	0.3 %	0.0 %	0.0 %	0.0 %
SE	Rel.	2.6 %	1.8 %	0.1 %	0.0 %	0.0 %	0.0 %	0.0 %
S		4.0 %	2.9 %	0.2 %	0.1 %	0.1 %	0.1 %	4.0 %
SW		52.0 %	43.8 %	16.3 %	8.1 %	5.7 %	5.6 %	52.0 %
NW		10.6 %	8.6 %	2.6 %	1.9 %	1.0 %	0.9 %	6.0 %

[1] Lakes with suitable temporal and radiometric characteristics for the automated lake ice break-up detection algorithm. [2] Lakes used for spatiotemporal analysis. [3] Lakes used for analysis of excess radiation, energy, and cumulative PDDs. [4] Lakes used for the upscaled results of excess energy.

Appendix B

Table B1. Lake ice break-up validation from time-lapse cameras (Abermann et al., 2019) in SW Greenland.

Year	Badesø			Langesø			Quassi-sø			Yearly mean error	Overall mean error
	Lake ID: 16515			Lake ID: 17830			Lake ID: 17831				
	13 m a.s.l.			21 m a.s.l			226 m a.s.l.				
	DOY val.	DOY S1	Diff.	DOY val.	DOY S1	Diff.	DOY val.	DOY S1	Diff.		
2017	168	169	1	167	168	1	173	175	2	1	5
2018	171	189	18	171	–	–	184	–	–	18	
2019	149	152	3	148	152	4	159	–	–	4	
2020	161	–	–	166	171	5	179	185	6	6	

Table B2. Lake ice break-up validation from observations, thermistor data, and satellite imagery of 11 lakes (Saros et al., 2019) in the Kangerlussuaq area compared to 14 lakes from our study close by.

Year	Median DOY val.	Median DOY S1	Diff.	Overall mean difference
2017	155	162	7	
2018	164	169	5	
2019	139	144	5	5
2020	150	154	4	
2021	150	153	3	

Table B3. Lake ice break-up validation from ESA CCI data (ESA, 2023a) in SW Greenland.

Year	Lake ID 70398			Lake ID 70316			Yearly mean error	Overall mean error
	519 m a.s.l.			707 m a.s.l				
	DOY val.	DOY S1	Diff.	DOY val.	DOY S1	Diff.		
2017	177	181	4	172	175	3	4	2
2018	199	199	0	199	201	2	1	
2019	160	165	5	159	160	1	3	
2020	182	184	2	183	184	1	2	

Appendix C

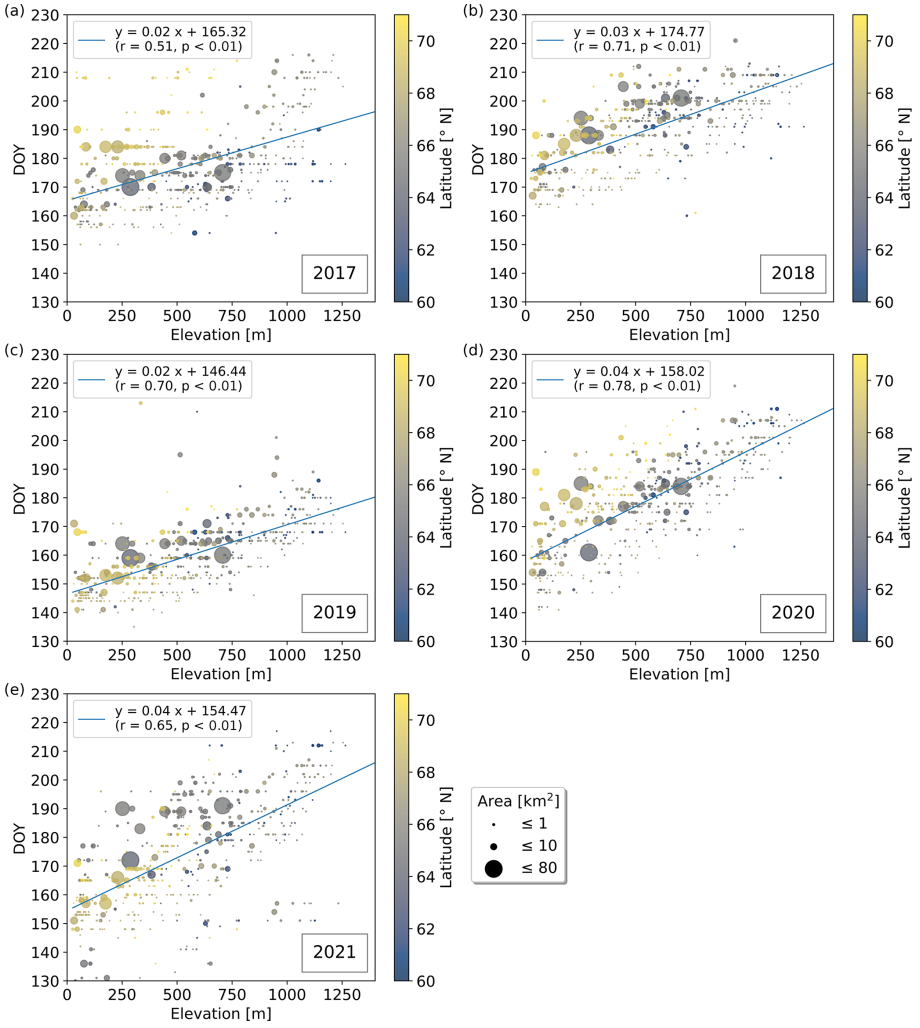

Figure C1. Lake ice break-up timings vs. elevation for the years **(a)** 2017 to **(e)** 2021. Break-up dates increase by 2–4 d per 100 m elevation gain, exhibiting strong correlations ($0.51 \leq r \leq 0.78$; $p<0.01$).

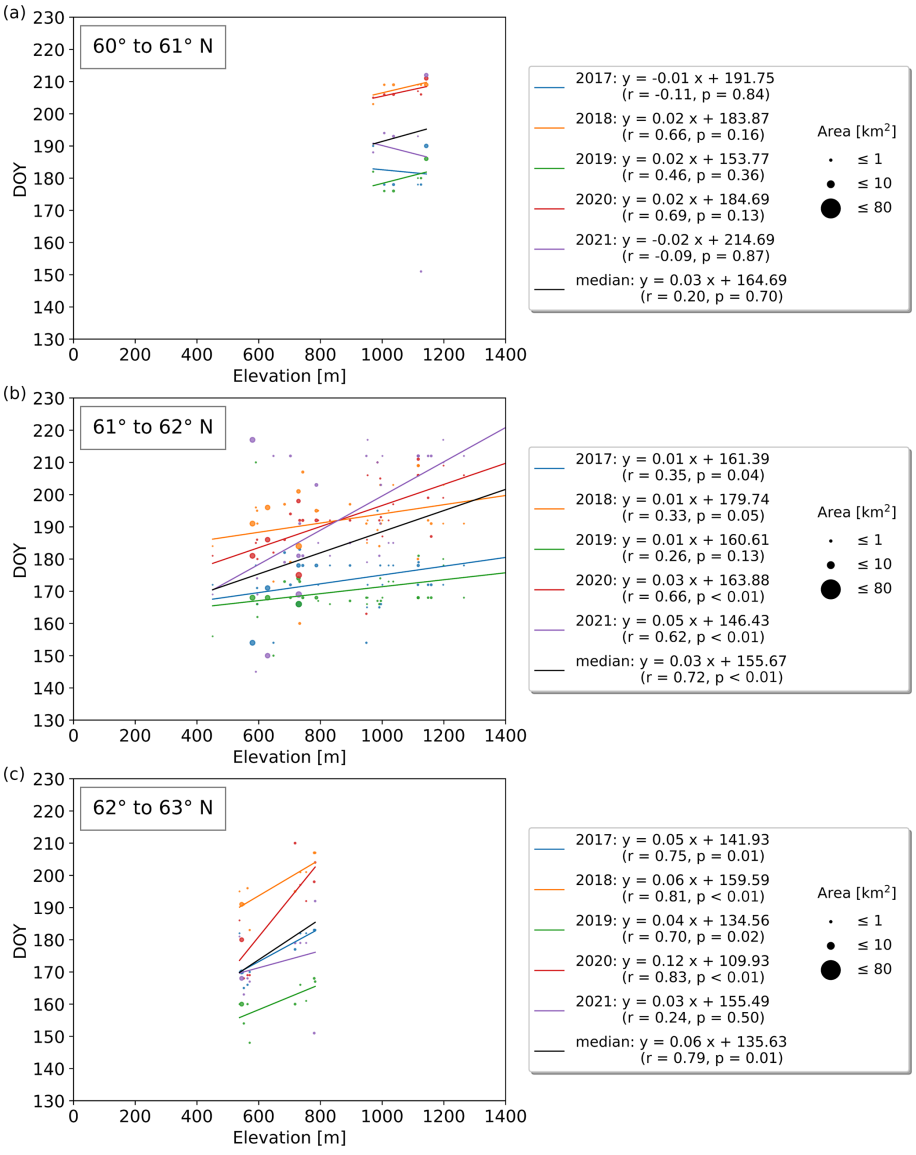

Figure C2. (a–c) Yearly lake ice break-up timings vs. elevation grouped by 1° latitude between 60 and 63° N. Several years exhibit strong correlations between break-up timing and elevation which increase by 3–6 d per 100 m elevation gain.

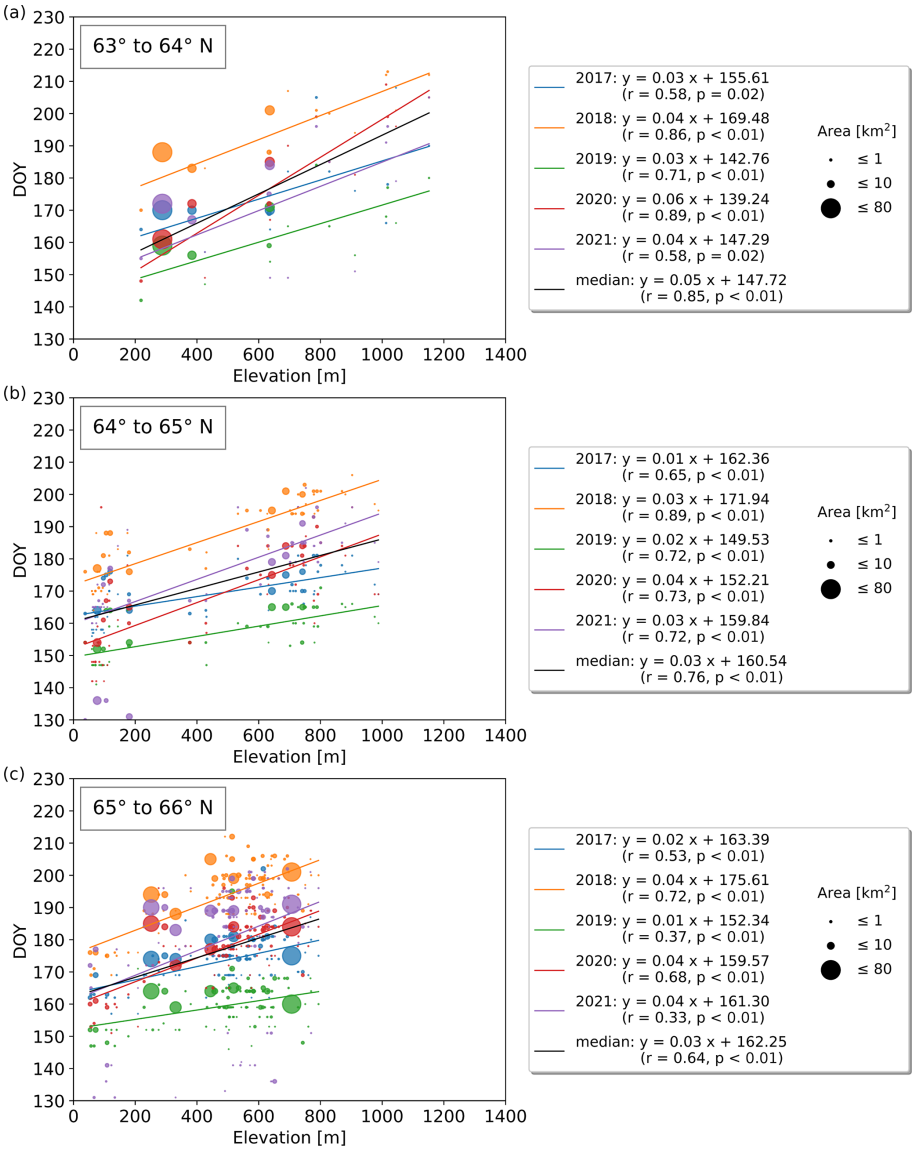

Figure C3. (a–c) Yearly lake ice break-up timings vs. elevation grouped by 1° latitude between 63 and 66° N. Several years exhibit strong correlations between break-up timing and elevation which increase by 3–6 d per 100 m elevation gain.

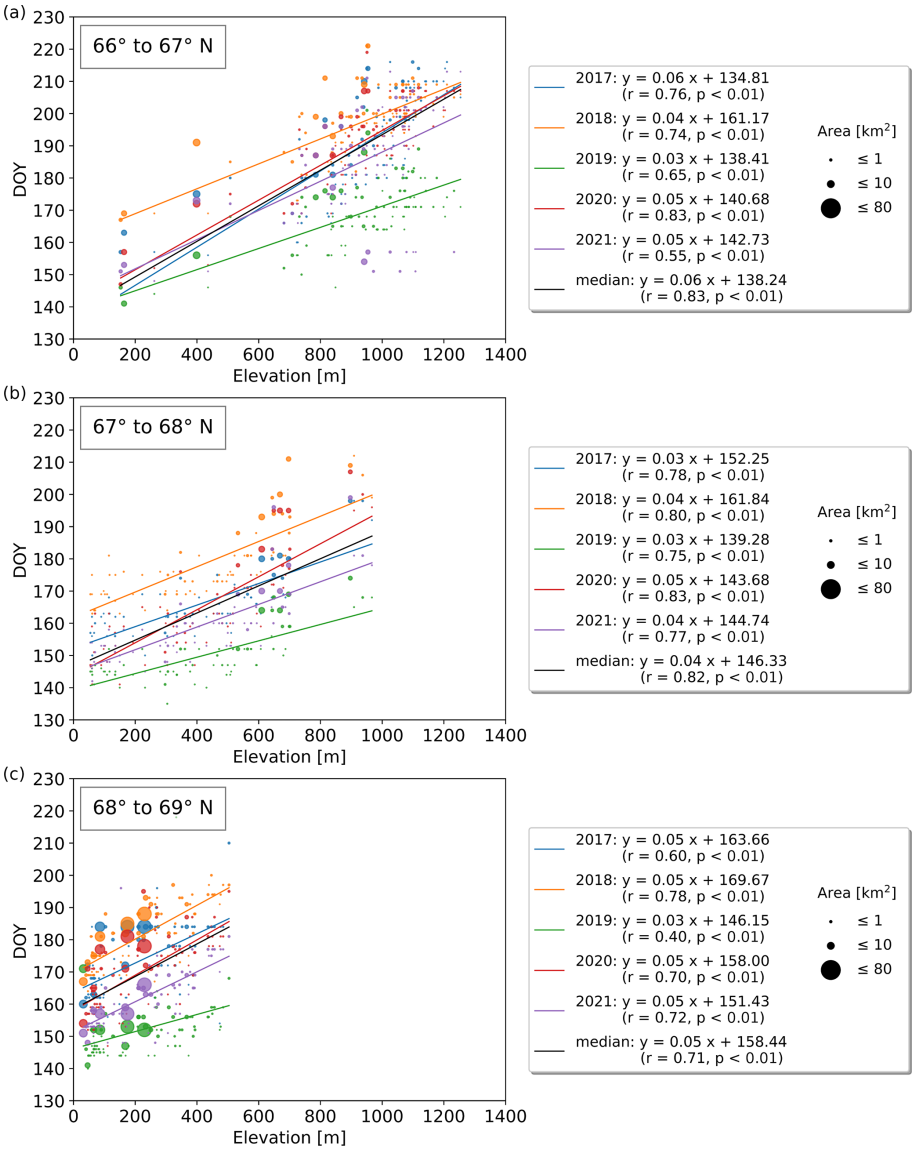

Figure C4. (a–c) Yearly lake ice break-up timings vs. elevation grouped by 1° latitude between 66 and 69° N. Several years exhibit strong correlations between break-up timing and elevation which increase by 3–6 d per 100 m elevation gain.

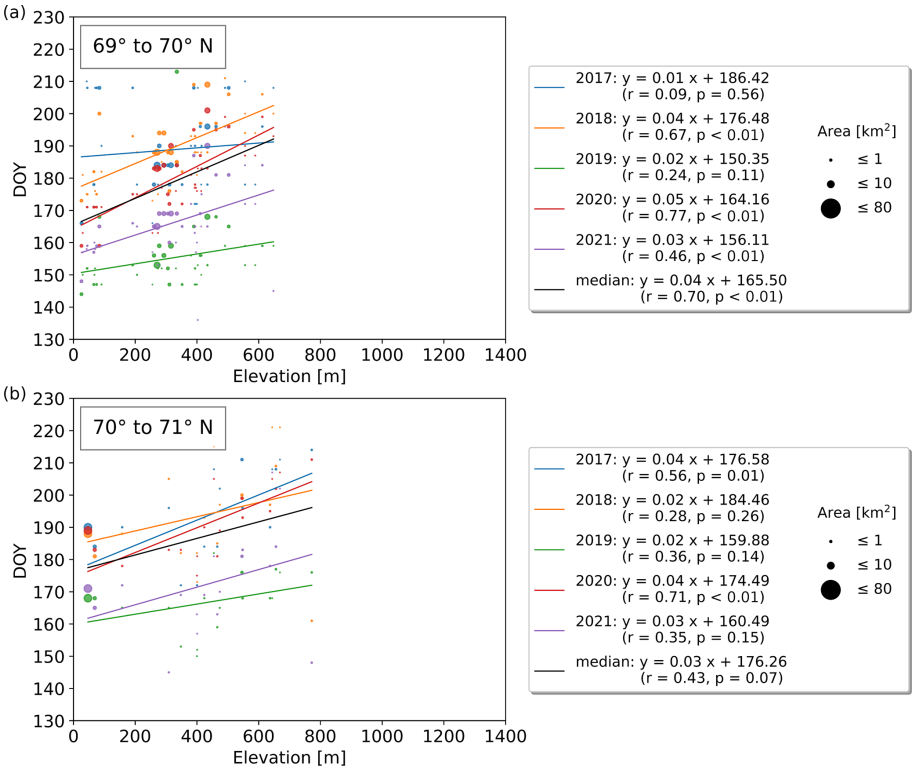

Figure C5. (a–c) Yearly lake ice break-up timings vs. elevation grouped by 1° latitude between 69 and 71° N. Several years exhibit strong correlations between break-up timing and elevation which increase by 3–5 d per 100 m elevation gain.

Table C1. Correlation characteristics of the relation between lake ice break-up timing and latitude, as well as between lake ice break-up timing and lake size. The number of N relations for assessing the number of n significant relations corresponds to the number of years (lake-specific annual break-up DOY vs. latitude/lake size), the number of elevation bands (lake-specific 2017–2021 median break-up DOY vs. latitude/lake size), the number of latitude bands (lake-specific 2017–2021 median break-up DOY vs. lake size), the years multiplied by the number of elevation bands (lake-specific annual break-up DOY and latitude/lake size grouped by elevation bands of 100 m), or the years multiplied by the number of latitude bands (lake-specific annual break-up DOY and lake size grouped by latitude bands of 1°). Correlation characteristics based on lake-specific 2017–2021 median break-up DOY, as well as the low number of significant relations in most cases, highlight the weak relationship between lake ice break-up timing and latitude or lake size.

Correlation between	Correlation coefficient r	Significance value p	Being significant ($p \leq 0.05$) in n/N relations
Lake-specific 2017–2021 median break-up DOY and latitude	-0.18	<0.01	1/1
Lake-specific 2017–2021 median break-up DOY and latitude (lakes grouped by elevation bands of 100 m)	$0.32 \leq r \leq 0.45$	≤ 0.05	7/13
Lake-specific annual break-up DOY and latitude	$-0.41 \leq r \leq 0.16$	<0.01	5/5
Lake-specific annual break-up DOY and latitude (lakes grouped by elevation bands of 100 m)	$-0.41 \leq r \leq 0.58$	≤ 0.05	21/65
Lake-specific 2017–2021 median break-up DOY and lake size	0.03	0.47	–
Lake-specific 2017–2021 median break-up DOY and lake size (lakes grouped by elevation bands of 100 m)	$0.25 \leq r \leq 0.58$	≤ 0.05	6/13
Lake-specific 2017–2021 median break-up DOY and lake size (lakes grouped by latitude bands of 1°)	0.50	0.05	1/11
Lake-specific annual break-up DOY and lake size	–	–	0/5
Lake-specific annual break-up DOY and lake size (lakes grouped by elevation bands of 100 m)	$-0.40 \leq r \leq 0.65$	≤ 0.05	25/65
Lake-specific annual break-up DOY and lake size (lakes grouped by latitude bands of 1°)	$-0.20 \leq r \leq 0.60$	≤ 0.05	5/55

Appendix D

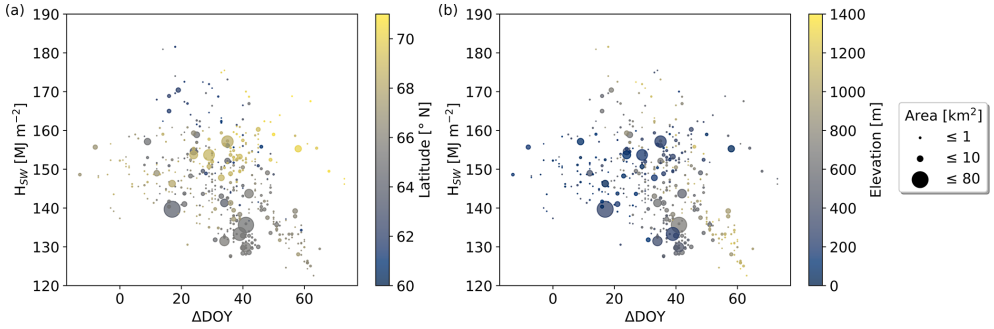

Figure D1. Excess radiation H_{SW} due to lake-specific break-up timings which are 8 d earlier compared to the median break-up timings for the period 2017 to 2021 vs. the time lag between the date of maximum incoming solar radiation and median lake ice break-up (ΔDOY), with color signatures for **(a)** latitude and **(b)** elevation. The median value of ΔDOY for the studied lakes amounts to 35 d (i.e., the lake-specific median break-up timing is 35 d after the solar radiation maximum).

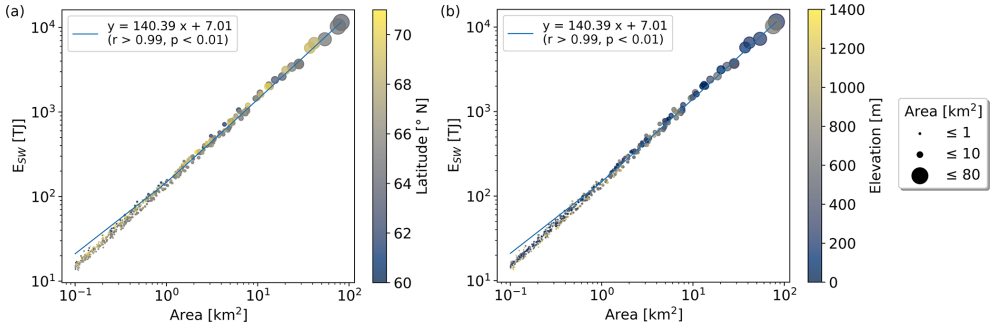

Figure D2. Excess energy E_{SW} due to lake-specific break-up timings which are 8 d earlier compared to the median break-up timings for the period 2017 to 2021 vs. lake surface area with color signatures for **(a)** latitude and **(b)** elevation. Lake surface areas strongly determine E_{SW} values explaining more than 99 % of the variability in E_{SW} (p<0.01).

Data availability. Data including the timing of lake ice break-up in Greenland and further results of our study are publicly available for download (https://doi.org/10.5281/zenodo.10577480, Posch et al., 2024).

Author contributions. CP developed the detection algorithm, processed the data, produced all results and plots, and drafted the paper. JA developed the idea and greatly determined the scope and direction of the study and results. TS contributed the climatological background and RACMO2.3p2 data to the study. All authors contributed suggestions to the paper.

Competing interests. The contact author has declared that none of the authors has any competing interests.

Disclaimer. Publisher's note: Copernicus Publications remains neutral with regard to jurisdictional claims made in the text, published maps, institutional affiliations, or any other geographical representation in this paper. While Copernicus Publications makes every effort to include appropriate place names, the final responsibility lies with the authors.

Acknowledgements. We thank Václava Hazuková and Jasmine Saros for providing observations on lake ice break-up dates for lakes in the Kangerlussuaq area (SW Greenland). Their data greatly contributed to validating our detection algorithm.

Financial support. This research has been supported by the University of Graz.

Review statement. This paper was edited by John Yackel and reviewed by two anonymous referees.

References

Abermann, J., Eckerstorfer, M., Malnes, E., and Hansen, B. U.: A large wet snow avalanche cycle in West Greenland quantified using remote sensing and in situ observations, Nat. Hazards, 97, 517–534, https://doi.org/10.1007/s11069-019-03655-8, 2019.

Abermann, J., Langley, K., Myreng, S. M., Rasmussen, K., and Petersen, D.: Heterogeneous timing of freshwater input into Kobbefjord, a low-arctic fjord in Greenland, Hydrol. Process., 35, e14413, https://doi.org/10.1002/hyp.14413, 2021.

Adrian, R., O'Reilly, C. M., Zagarese, H., Baines, S. B., Hessen, D. O., Keller, W., Livingstone, D. M., Sommaruga, R., Straile, D., Van Donk, E., Weyhenmeyer, G. A., and Winderl, M.: Lakes as sentinels of climate change, Limnol Oceanogr., 54, 2283–2297, https://doi.org/10.4319/lo.2009.54.6_part_2.2283, 2009.

Bales, R. C., Guo, Q., Shen, D., McConnell, J. R., Du G., Burkhart, J. F., Spikes, V. B., Hanna, E., and Cappelen, J.: Annual accumulation for Greenland updated using ice core data developed during 2000–2006 and analysis of daily coastal meteorological data, J. Geophys. Res., 114, D06116, https://doi.org/10.1029/2008JD011208, 2009.

Ballinger, T. J., Hanna, E., Hall, R. J., Carr, J. R., Brasher, S., Osterberg, E. C., Capellen, J., Tedesco, M., Ding, Q., and Mernild, S. H.: The role of blocking circulation and emerging open water feedbacks on Greenland cold-season air temperature variability over the last century, Int. J. Climatol., 41, E2778–E2800, https://doi.org/10.1002/joc.6879, 2020.

Box, J. E., Wehrlé, A., van As, D., Fausto, R. S., Kjeldsen, K. K., Dachauer, A., Ahlstrøm, P. A., and Picard, G.: Greenland ice sheet rainfall, heat and albedo feedback impacts from the mid-August 2021 atmospheric River, Geophys. Res. Lett., 49, e2021GL097356, https://doi.org/10.1029/2021GL097356, 2022.

Box, J. E., Nielsen, K. P., Yang, X., Niwano, M., Wehrlé, A., van As, D., Fettweis, X., Køltzow, M. A. Ø., Palmason, B., Fausto, R. S., van den Broeke, M. R., Huai, B., Ahlstrøm, A. P., Langley, K., Dachauer, A., and Noël, B.: Greenland ice sheet rainfall climatology, extremes and atmospheric river rapids, Meteorol. Appl., 30, e2134, https://doi.org/10.1002/met.2134, 2023.

Brown, L. C. and Duguay, C. R.: The response and role of ice cover in lake-climate interactions, Prog. Phys. Geog., 34, 671–704, https://doi.org/10.1177/0309133310375653, 2010.

Cherry, J. E., Knapp, C., Trainor, S., Ray, A. J., Tedesche, M., and Walker, S.: Planning for climate change impacts on hydropower in the Far North, Hydrol. Earth Syst. Sci., 21, 133–151, https://doi.org/10.5194/hess-21-133-2017, 2017.

Delaunay, B. N.: Sur la sphère vide, Bulletin of Academy of Sciences of the USSR, 7, 793–800, 1934.

Duguay, C. R., Prowse, T. D., Bonsal, B. R., Brown, R. D., Lacroix, M. P., and Ménard, P.: Recent trends in Canadian lake ice cover, Hydrol. Process., 20, 781–801, https://doi.org/10.1002/hyp.6131,2006.

Duguay, C. R., Bernier, M., Gauthier, Y., and Kouraev, A.: Remote sensing of lake and river ice, in: Remote Sensing of the Cryosphere, First Edition, edited by: Tedesco, M., John Wiley & Sons, Hoboken, New Jersey, 273–306, https://doi.org/10.1002/9781118368909.ch12, 2015.

Ettema, J., van den Broeke, M. R., van Meijgaard, E., and van de Berg, W. J.: Climate of the Greenland ice sheet using a high-resolution climate model – Part 2: Near-surface climate and energy balance, The Cryosphere, 4, 529–544, https://doi.org/10.5194/tc-4-529-2010, 2010.

European Space Agency (ESA): Climate Change Initiative Lakes, https://climate.esa.int/en/projects/lakes, last access: 23 June 2023a.

European Space Agency (ESA): Sentinel-1 SAR User Guide, https://sentinel.esa.int/web/sentinel/user-guides/sentinel-1-sar, last access: 16 April 2023b.

European Space Agency (ESA): Sentinel-1, https://sentinel.esa.int/web/sentinel/missions/sentinel-1, last access: 16 April 2023c.

European Space Agency (ESA): The Sentinel-1 Toolbox, https://sentinel.esa.int/web/sentinel/toolboxes/sentinel-1, last access: 26 June 2023d.

European Space Agency (ESA): Sentinel-1 SAR Technical Guide, https://sentinels.copernicus.eu/web/sentinel/technical-guides/sentinel-1-sar, last access: 16 April 2023e.

European Space Agency (ESA): Sentinel-1 Algorithms, https://developers.google.com/earth-engine/guides/sentinel1#metadata-and-filtering, last access: 26 June 2023f.

Fettweis, X., Box, J. E., Agosta, C., Amory, C., Kittel, C., Lang, C., van As, D., Machguth, H., and Gallée, H.: Reconstructions of the 1900–2015 Greenland ice sheet surface mass balance using the regional climate MAR model, The Cryosphere, 11, 1015–1033, https://doi.org/10.5194/tc-11-1015-2017, 2017.

Gebre, S., Alfredsen, K., Lia, L., Stickler, M., Tesaker, E.: Review of Ice Effects on Hydropower Systems, J. Cold Reg. Eng., 27, 196–222, https://doi.org/10.1061/(ASCE)CR.1943-5495.0000059, 2013.

Google Inc.: Earth Engine Code Editor, https://code.earthengine.google.com, last access: 16 April 2023a.

Google Inc.: Earth Engine Data Catalogue, https://developers.google.com/earth-engine/datasets, last access: 16 April 2023b.

Hallerbäck, S., Huning, L. S., Love, C., Persson, M., Stensen, K., Gustafsson, D., and AghaKouchak, A.: Climate warming shortens ice durations and alters freeze and break-up patterns in Swedish water bodies, The Cryosphere, 16, 2493–2503, https://doi.org/10.5194/tc-16-2493-2022, 2022.

Hanna, E., Capellen, J., Fettweis, X., Mernild, S. H., Mote, T. L., Mottram, R., Steffen, K., Ballinger, T. J., and Hall, R. J.: Greenland surface air temperature changes from 1981 to 2019 and implications for ice-sheet melt and mass-balance change, Int J. Climatol., 41, 1336–1352, https://doi.org/10.1002/joc.6771, 2021.

Hock, R., Maussion, F., Marzeion, B., and Nowicki, S.: What is the global glacier ice volume outside the ice sheets?, J. Glaciol., 69, 273, 204–210, https://doi.org/10.1017/jog.2023.1, 2023.

Huai, B., van den Broeke, M. R., Reijmer, C H., and Noël, B.: A daily 1-km resolution Greenland rainfall climatology (1958–2020) from statistical downscaling of a regional atmospheric climate model, J. Geophys. Res.-Atmos., 127, e2022JD036688, https://doi.org/10.1029/2022JD036688, 2022.

Huang, L., Timmermann, A., Lee, S.-S., Rodgers, K. B., Yamaguchi, R., and Chung, E.-S.: Emerging unprecedented lake ice loss in climate change projections, Nat. Commun., 13, 5798, https://doi.org/10.1038/s41467-022-33495-3, 2022.

Imrit, M. A. and Sharma, S.: Climate Change is Contributing to Faster Rates of Lake Ice Loss in Lakes Around the Northern Hemisphere, J. Geophys. Res.-Biogeo., 126, e2020JG006134, https://doi.org/10.1029/2020JG006134, 2021.

IPCC: Climate Change 2023: Synthesis Report. Contribution of Working Groups I, II and III to the Sixth Assessment Report of the Intergovernmental Panel on Climate Change, IPCC, Geneva, Switzerland, 35–115, https://doi.org/10.59327/IPCC/AR6-9789291691647, 2023.

Jeffries, M. O., Morris, K., and Duguay, C. R.: Floating ice: lake ice and river ice, in: Satellite Image Atlas of Glaciers of the World – State of the Earth's Cryosphere at the Beginning of the 21st Century: Glaciers, Global Snow Cover, Floating Ice, and Permafrost and Periglacial Environments, edited by: Williams, R. S. and Ferrigno, J. G., U.S. Geological Survey, Reston, Virginia, A381–A424, https://doi.org/10.3133/pp1386, 2012.

Jiang, S., Ye, A., and Xiao, C.: The temperature increase in Greenland has accelerated in the past five years, Global Planet. Change, 194, 103297, https://doi.org/10.1016/j.gloplacha.2020.103297, 2020.

Karami, M., Hansen, B. U., Westergaard-Nielsen, A., Abermann, J., Lund, M., Schmidt, N. M., and Elberling, B.: Vegetation phenology gradients along the west and east coasts of Greenland from 2001 to 2015, Ambio, 46, 94–105, https://doi.org/10.1007/s13280-016-0866-6, 2017.

Koenig, L. S., Ivanoff, A., Alexander, P. M., MacGregor, J. A., Fettweis, X., Panzer, B., Paden, J. D., Forster, R. R., Das, I., McConnell, J. R., Tedesco, M., Leuschen, C., and Gogineni, P.: Annual Greenland accumulation rates (2009–2012) from airborne snow radar, The Cryosphere, 10, 1739–1752, https://doi.org/10.5194/tc-10-1739-2016, 2016.

Korhonen, J.: Long-term changes in lake ice cover in Finland, Nordic Hydrology, 37, 347–363, https://doi.org/10.2166/nh.2006.019, 2006.

L'Abée-Lund, J. H., Vøllestad, L. A., Brittain, J. E., Kvambekk, Å. S., and Solvang, T.: Geographic variation and temporal trends in ice phenology in Norwegian lakes during the period 1890–2020, The Cryosphere, 15, 2333–2356, https://doi.org/10.5194/tc-15-2333-2021, 2021.

Lindenschmidt, K. E., van der Sanden, J., Demski, A., Drouin, H., and Geldsetzer, T.: Characterising river ice along the Lower Red River using RADARSAT-2 imagery, in: CGU HS Committee on River Ice Processes and the Environment, 16th Workshop on River Ice, Winnipeg, Manitoba, 18–22 September 2011, 1–16, 2011.

Magnuson, J. J., Robertson, D. M., Benson, B. J., Wynne, R. H., Livingstone, D. M., Arai, T., Assel, R. A., Barry, R. G., Card V., Kuusisto, E., Granin, N. G., Prowse, T. D., Stewart, K. M., and Vuglinski, V. S.: Historical Trends in Lake and River Ice Cover in the Northern Hemisphere, Science, 289, 1743–1746, https://doi.org/10.1126/science.289.5485.1743, 2000.

Mankoff, K. D., Fettweis, X., Langen, P. L., Stendel, M., Kjeldsen, K. K., Karlsson, N. B., Noël, B., van den Broeke, M. R., Solgaard, A., Colgan, W., Box, J. E., Simonsen, S. B., King, M. D., Ahlstrøm, A. P., Andersen, S. B., and Fausto, R. S.: Greenland ice sheet mass balance from 1840 through next week, Earth Syst. Sci. Data, 13, 5001–5025, https://doi.org/10.5194/essd-13-5001-2021, 2021.

Moreira, A., Prats-Iraola, P., Younis, M., Krieger, G., Hajnsek, I., and Papathanassiou, K. P.: A tutorial on synthetic aperture radar, IEEE Geoscience and Remote Sensing Magazine, 1, 6–43, https://doi.org/10.1109/MGRS.2013.2248301, 2013.

Murfitt, J. and Duguay, C. R.: Assessing the Performance of Methods for Monitoring Ice Phenology of the World's Largest High Arctic Lake Using High-Density Time Series Analysis of Sentinel-1 Data, Remote Sens., 12, 3, 382, https://doi.org/10.3390/rs12030382, 2020.

Murfitt, J. and Duguay, C. R.: 50 years of lake ice research from active microwave remote sensing: Progress and prospects, Remote Sens. Environ., 264, 112616, https://doi.org/10.1016/j.rse.2021.112616, 2021.

Noël, B., van de Berg, W. J., Lhermitte, S., and van den Broeke, M. R.: Rapid ablation zone expansion amplifies north Greenland mass loss, Science Advances, 5, eaaw0123, https://doi.org/10.1126/sciadv.aaw0123, 2019.

Posch, C., Abermann, J., and Silva, T.: Lake Ice Break-Up across Peripheral Greenland (2017–2021) from Sentinel-1 SAR, Zenodo [data set], https://doi.org/10.5281/zenodo.10577480, 2024.

Prowse, T., Alfredsen, K., Beltaos, S., Bonsal, B. R., Bowden, W. B., Duguay, C. R., Korhola, A., McNamara, J., Vincent, W. F., Vuglinsky, V., Walter Anthony, K. M., and Weyhenmeyer, G. A.: Effects of Changes in Arctic Lake and River Ice, Ambio, 40, 63–74, https://doi.org/10.1007/s13280-011-0217-6, 2011.

Saros, J. E., Anderson, N. J., Juggins, S., McGowan, S., Yde, J. C., Telling, J., Bullard, J. E., Yallop, M. L., Heathcote, A. J., and Burpee, B. T.: Arctic climate shifts drive rapid ecosystem responses across the West Greenland landscape, Environ. Res. Lett., 14, 074027, https://doi.org/10.1088/1748-9326/ab2928, 2019.

Shen, D., Liu, Y., and Huang, S.: Annual accumulation over the greenland ice sheet interpolated from historical and newly compiled observation data, Geogr. Ann. A, 94, 377–393, https://doi.org/10.1111/j.1468-0459.2012.00458.x, 2012.

Siles, G., Leconte, R., and Peters D. L.: Retrieval of Lake Ice Characteristics from SAR Imagery, Can. J. Remote Sens., 48, 379–399, https://doi.org/10.1080/07038992.2022.2042227, 2022.

Silva, T., Abermann, J., Noël, B., Shahi, S., van de Berg, W. J., and Schöner, W.: The impact of climate oscillations on the surface energy budget over the Greenland Ice Sheet in a changing climate, The Cryosphere, 16, 3375–3391, https://doi.org/10.5194/tc-16-3375-2022, 2022.

Slater, T., Shepherd, A., McMillan, M., Leeson, A., Gilbert, L., Muir, A., Munneke, P. K., Noël, B., Fettweis, X., van den Broeke, M., and Briggs, K.: Increased variability in Greenland Ice Sheet runoff from satellite observations, Nat. Commun., 12, 6069, https://doi.org/10.1038/s41467-021-26229-4, 2021.

Stonevicius, E., Uselis, G., and Grendaite, D.: Ice Detection with Sentinel-1 SAR Backscatter Threshold in Long Sections of Temperate Climate Rivers, Remote Sensing, 14, 1627, https://doi.org/10.3390/rs14071627, 2022.

Styrelsen for Dataforsyning og Infrastruktur: Åbent Land Grønland, Dataforsyningen [data set], https://dataforsyningen.dk/data/4771, last access: 26 June 2023a.

Styrelsen for Dataforsyning og Infrastruktur: Databoks Grønland, https://dataforsyningen.dk/data, last access: 26 June 2023b.

Tom, M., Aguilar, R., Imhof, P., Leinss, S., Baltsavias, E., and Schindler, K.: Lake Ice Detection from Sentinel-1 SAR With

Deep Learning, ISPRS Ann. Photogramm. Remote Sens. Spatial Inf. Sci., V-3-2020, 409–416, https://doi.org/10.5194/isprs-annals-V-3-2020-409-2020, 2020.

United Nations: Transforming our world: The 2030 Agenda for Sustainable Development, https://sdgs.un.org/publications/transforming-our-world-2030-agenda-sustainable-development-17981 (last access: 26 June 2023), 2015.

Unterschultz, K. D., van der Sanden, J., and Hicks, F. E.: Potential of RADARSAT-1 for the monitoring of river ice: Results of a case study on the Athabasca River at Fort McMurray, Canada, Cold Reg. Sci. Technol., 5, 238–248, https://doi.org/10.1016/j.coldregions.2008.02.003, 2009.

U.S./Japan ASTER Science Team: ASTGTM v003, ASTER Global Digital Elevation Model 1 arc second, Land Processes Distributed Active Archive Center [data set], https://doi.org/10.5067/ASTER/ASTGTM.003, 2023.

van der Schot, J., Abermann, J., Silva, T., Jensen, C. D., Noël, B., and Schöner, W.: Precipitation trends (1958–2021) on Ammassalik island, south-east Greenland, Front. Earth Sci., 10, 1085499, https://doi.org/10.3389/feart.2022.1085499, 2023.

Wang, J., Duguay, C. R., Clausi, D. A., Pinard, V., and Howell, S. E. L.: Semi-Automated Classification of Lake Ice Cover Using Dual Polarization RADARSAT-2 Imagery, Remote Sens., 10, 1727, https://doi.org/10.3390/rs10111727, 2018.

Westergaard-Nielsen, A., Karami, M., Hansen, B. U., Westermann, S., and Elberling, B.: Contrasting temperature trends across the ice-free part of Greenland, Scientific Reports 8, 1586, https://doi.org/10.1038/s41598-018-19992-w, 2018.

Westergaard-Nielsen, A., Hansen, B. U., Elberling, B., and Abermann, J.: Greenland Climates, in: Encyclopedia of the World's Biomes, edited by: Goldstein, M. I., and DellaSalla, D. A., Elsevier, Amsterdam, Netherlands, 539–550, https://doi.org/10.1016/B978-0-12-409548-9.11750-6, 2020.

Weyhenmeyer, G. A., Meili, M., and Livingstone, D. M.: Nonlinear temperature response of lake ice breakup, Geophys. Res. Lett., 31, L07203, https://doi.org/10.1029/2004GL019530, 2004.

Williams, G., Layman, K. L., Stefan, H. G.: Dependence of lake ice covers on climatic, geographic and bathymetric variables, Cold Reg. Sci. Technol., 40, 145–164, https://doi-org/10.1016/j.coldregions.2004.06.010, 2004.

Williams, G. and Stefan, H. G.: Modeling of Lake Ice Characteristics in North America Using Climate, Geography, and Lake Bathymetry, J. Cold Reg. Eng., 20, 140–167, https://doi-org/10.1061/(asce)0887-381x(2006)20:4(140), 2006.

Woolway, R. I., Kraemer, B. M., Lenters, J. D., Merchant, C. J., O'Reilly, C. M., and Sharma, S.: Global lake responses to climate change, Nat. Rev. Earth Environ., 1, 388–403, https://doi.org/10.1038/s43017-020-0067-5, 2020.

World Meteorological Organization (WMO): The 2022 GCOS Implementation Plan (GCOS-244), https://library.wmo.int/records/item/58104-the-2022-gcos-implementation-plan-gcos-244, last access: 26 June 2023a.

World Meteorological Organization (WMO): The 2022 GCOS ECVs Requirements (GCOS 245), https://library.wmo.int/records/item/58111-the-2022-gcos-ecvs-requirements-gcos-245, last access: 26 June 2023b.

Zhang, S., Pavelsky, T. M., Arp, C. D., and Yang, X.: Remote sensing of lake ice phenology in Alaska, Environ. Res. Lett., 16, 064007, https://doi.org/10.1088/1748-9326/abf965, 2021.